


Evaluation of Neural Regulation and Microglial Responses to Brain Injury in Larval Zebrafish Exposed to Perfluorooctane Sulfonate

Shannon E. Paquette,¹ Nathan R. Martin,¹ April Rodd,¹ Katherine E. Manz,² Eden Allen,¹ Manuel Camarillo,¹ Hannah I. Weller,³ Kurt Pennell,² and Jessica S. Plavicki¹ 

¹Department of Pathology and Laboratory Medicine, Brown University, Providence, Rhode Island, USA

²School of Engineering, Brown University, Providence, Rhode Island, USA

³Department of Ecology, Evolution, and Organismal Biology, Brown University, Providence, Rhode Island, USA

BACKGROUND: Per- and polyfluoroalkyl substances (PFAS) are biopersistent, global pollutants. Although some *in vitro* and epidemiological studies have explored the neurotoxic potential of perfluorooctane sulfonate (PFOS), a prevalent PFAS congener, it is unknown how developmental PFOS exposure affects neuronal signaling, microglia development, and microglial–neuron communication.

OBJECTIVES: We sought to determine the extent to which PFOS exposure disrupts brain health, neuronal activity, and microglia–neuron communication during development. In addition, although PFOS impairs humoral immunity, its impact on innate immune cells, including resident microglia, is unclear. As such, we investigated whether microglia are cellular targets of PFOS, and, if so, whether disrupted microglial development or function could contribute to or is influenced by PFOS-induced neural dysfunction.

METHODS: Zebrafish were chronically exposed to either a control solution [0.1% dimethyl sulfoxide (DMSO)], 7 μ M PFOS, 14 μ M PFOS, 28 μ M PFOS, or 64 μ M perfluorooctanoic acid (PFOA). We used *in vivo* imaging and gene expression analysis to assess microglial populations in the developing brain and to determine shifts in the microglia state. We functionally challenged microglia state using a brain injury model and, to assess the neuronal signaling environment, performed functional neuroimaging experiments using the photoconvertible calcium indicator calcium-modulated photoactivatable ratiometric integrator (CaMPARI). These studies were paired with optogenetic manipulations of neurons and microglia, an untargeted metabolome-wide association study (MWAS), and behavioral assays.

RESULTS: Developmental PFOS exposure resulted in a shift away from the homeostatic microglia state, as determined by functional and morphological differences in exposed larvae, as well as up-regulation of the microglia activation gene *p2ry12*. PFOS-induced effects on microglia state exacerbated microglia responses to brain injury in the absence of increased cell death or inflammation. PFOS exposure also heightened neural activity, and optogenetic silencing of neurons or microglia independently was sufficient to normalize microglial responses to injury. An untargeted MWAS of larval brains revealed PFOS-exposed larvae had neurochemical signatures of excitatory–inhibitory imbalance. Behaviorally, PFOS-exposed larvae also exhibited anxiety-like thigmotaxis. To test whether the neuronal and microglial phenotypes were specific to PFOS, we exposed embryos to PFOA, a known immunotoxic PFAS. PFOA did not alter thigmotaxis, neuronal activity, or microglial responses, further supporting a role for neuronal activity as a critical modifier of microglial function following PFOS exposure.

DISCUSSION: Together, this study provides, to our knowledge, the first detailed account of the effects of PFOS exposure on neural cell types in the developing brain *in vivo* and adds neuronal hyperactivity as an important end point to assess when studying the impact of toxicant exposures on microglia function. <https://doi.org/10.1289/EHP12861>

Introduction

Pollution poses a global threat to environmental, ecologic, and economic health and stability. As international geologic committees consider whether we have now entered the Anthropocene Age, it is of increasing importance to understand the broad impacts of human-made pollutants. It is also worth emphasizing that the burden of pollution is disproportionately shared, with minority and low-income communities being more susceptible to the physical consequences of insufficient regulatory laws, industrial waste disposal, and air pollution.^{1–3} If we are to protect our health, society, and environment, more research efforts are needed to address the costs of our past and present environmental negligence.

One major class of chemicals of increasing concern are per- and polyfluoroalkyl substances (PFAS). Although PFAS were

only introduced in industrial manufacturing in the mid-20th century, the expansive and international use of PFAS has led to near universal exposure in humans.^{4,5} PFAS congeners are found in fire-fighting foams, commercial household products, such as water-repellant fabrics, food packaging, and nonstick finishes, and are used in a variety of applications in the aerospace, aviation, and automotive industries.⁶ Structurally, PFAS consist of fully or polyfluorinated aliphatic substances of varying carbon chain length and head groups, with longer chain length tending to be associated with increased toxicity.^{7–9} The strength of carbon–fluorine bonds lends most PFAS to be biopersistent, bioaccumulative, and resistant to degradation.¹⁰ As such, PFAS have acquired the disconcerting moniker of forever chemicals.

Of the >4,700 PFAS congeners,⁶ one of the most environmentally prevalent and extensively studied is perfluorooctane sulfonate (PFOS).¹⁰ PFOS has an 8-carbon chain with a sulfonic acid head group and has been associated with adverse outcomes related to the functioning and health of several major organ systems in humans¹¹ and animals,^{11,12} and is considered a metabolic, endocrine, and immune disruptor.^{13–19} *In utero* and developmental exposure to PFOS has particularly concerning consequences on adaptive immunity. Grandjean et al. demonstrated in humans that elevated PFOS levels in infancy and early childhood significantly attenuated adaptive immune responses, curbed antibody production, and limited vaccine efficacy.^{20,21} Such studies reinforce the necessity of understanding the impact of pollution on population health, especially considering the need to vaccinate individuals against emerging or evolving pathogens. PFOS-induced humoral immune disruption^{14,22} prompted the National Toxicology Program to

Address correspondence to Jessica S. Plavicki, Department of Pathology and Laboratory Medicine, Brown University, 70 Ship St., Providence, RI 02903 USA. Email: jessica_plavicki@brown.edu

Supplemental Material is available online (<https://doi.org/10.1289/EHP12861>).

The authors have no conflicts of interest to declare.

Received 7 February 2023; Revised 6 October 2023; Accepted 16 October 2023; Published 15 November 2023.

Note to readers with disabilities: *EHP* strives to ensure that all journal content is accessible to all readers. However, some figures and Supplemental Material published in *EHP* articles may not conform to 508 standards due to the complexity of the information being presented. If you need assistance accessing journal content, please contact ehpsubmissions@niehs.nih.gov. Our staff will work with you to assess and meet your accessibility needs within 3 working days.

classify PFOS as a “presumed immune hazard to humans” in 2016.²³ However, studies performed *in vitro* and in mice indicate the effects of PFOS on innate immunity are still largely inconclusive, with some groups finding that PFOS dampens innate cell infiltration, gene expression, or activity,^{24–26} and others describing heightened inflammation or immune function.^{27–29} Even less understood is the tissue-specific impact of PFOS on local immune populations, namely tissue-resident macrophages. Tissue-resident macrophages are largely yolk-sac or fetal liver-derived, heterogeneous, and, most notably, carry out discrete, noncanonical tissue-specific functions essential for development and homeostasis.³⁰ Determining whether tissue-resident macrophages are PFAS targets, especially during development, is essential for our understanding of long-term consequences of macrophage dysregulation following PFAS exposure.

In this work, we focus on microglia, the resident immune population of the central nervous system (CNS), as a potential PFOS target. Beyond effector immune responses, microglia have a highly dynamic and diverse repertoire of homeostatic functions, including developmental pruning of extra-numerary synapses,^{31,32} facilitating synaptogenesis and maturation,³³ and regulation of neural plasticity and dendritic spine density through frequent synaptic monitoring.^{34–36} As sentinels of the CNS, these persistent, self-renewing cells are also highly sensitive and rapidly adaptable to any changes in their environment.

Microglial dysfunction has been well documented in disease models of various neuropathological states, including Down syndrome,³⁷ Alzheimer’s disease,³⁸ and epilepsy.³⁹ Owing to the critical regulatory roles of microglia in neural health and development, there has been a concerted effort to clarify the mechanisms of bidirectional crosstalk between neurons and microglia.³⁵ However, the impact of environmental exposures on microglia–neuron interactions during developmentally sensitive periods of life, including gestation, has been largely overlooked. Some epidemiological studies suggested correlations between developmental PFOS exposure and attention-deficit/hyperactivity disorder (ADHD) incidence,^{40,41} whereas others found no such relationship.^{42–45} Meanwhile in mice, a single neonatal PFOS exposure was sufficient to alter proteins required for neuronal growth and synaptogenesis, in addition to causing spontaneous behavior and hyperactivity in adults.^{46,47} Developmental exposure to PFOS was also shown to cause hyperactive locomotor activity in larval zebrafish.^{48–50} *In vitro* experiments using cultured neurons revealed that PFOS interacts with inositol 1,4,5-triphosphate receptors (IP₃Rs) and ryanodine receptors (RyRs), leading to the release of intracellular calcium stores, which suggests a potential role for calcium in PFOS-induced neurotoxicity.⁵¹ However, it is still not known whether the induced locomotor activity in zebrafish is attributed to neuronal hyperactivity or skeletal muscle calcium utilization.⁵² It is also not known whether potential changes in the neuronal environment following PFOS exposure can impact microglia function, and vice versa.

Herein, we used the versatility, transparency, and *ex vivo* development of the larval zebrafish model to determine how chronic PFOS exposure impacts microglial and neuronal function *in vivo* during development. We employed a brain injury model, functional neuroimaging, larval behavioral assays, optogenetic modulation of cell-specific membrane potential, a metabolome-wide association study (MWAS), and a microglia knockout model in larval zebrafish to provide the first *in vivo* account of PFOS-induced disruption of microglial and neuronal activity. We also exposed larvae to a nonexcitatory PFAS congener, perfluorooctanoic acid (PFOA), to determine whether structurally similar compounds can have distinct effects on CNS health and neural cell function.

Materials and Methods

Zebrafish Husbandry

Zebrafish (*Danio rerio*) maintenance and experimental procedures were approved by the Brown University Institutional Animal Care and Use Committee (IACUC; 19-12-0003) adhering to the National Institutes of Health (NIH) “*Guide for the Care and Use of Laboratory Animals*.”⁵³ Zebrafish colonies were maintained in an aquatic housing system (Aquaneering Inc.), maintaining water temperature ($28.5 \pm 2^\circ\text{C}$), filtration, and purification, as well as automatic pH and conductivity stabilization, and ultraviolet (UV) irradiation disinfection. Adult and larval zebrafish were sustained in a 14:10 h light/dark cycle.⁵⁴ Adult zebrafish were fed once a day with GEMMA Micro (Skretting).

Adult zebrafish (of varying ages >3 months postfertilization) were placed into 1.7-L sloped spawning tanks (Techniplast) 15–18 h prior to mating. Sexes were separated by a transparent partition. Within 2 h of light cycle onset, the partition was removed, and zebrafish were allowed to spawn for 1 h. Embryos were collected in fresh egg water (60-mg/L Instant Ocean Sea Salts; Aquarium Systems) and placed into 100-mm nontreated culture petri dishes (CytoOne, Cat. No. CC7672-3394). Embryonic and larval zebrafish were maintained at $28.5 \pm 1^\circ\text{C}$ in an incubator (Powers Scientific Inc.) for up to 120 h postfertilization (hpf).

Zebrafish Lines

The following zebrafish lines were used in this study, either independently or in combination. To visualize green fluorescent macrophages, we used *Tg(mpeg1:EGFP)*⁵⁵ zebrafish. To modulate cellular membrane potential by inducing chloride ion influx, we used the optogenetic line halorhodopsin, which is a light-gated chloride pump that is sensitive to 589-nm light.^{56,57} This third-generation opsin exhibits reliable membrane trafficking for uniform surface expression, is resistant to inactivation, and has step-like, potent photocurrents that are stable over long timescales.⁵⁷ Halorhodopsin was under the control of a Gal4-regulated upstream activating sequence (UAS) for cell-specific control, *Tg(UAS:eNpHR3.0-mCherry)*.^{56,57} To detect calcium activity in neurons *in vivo*, we used a transgenic line with neuron-specific expression of the calcium sensor calcium-modulated photoactivatable ratio-metric integrator (CaMPARI) under the pan-neuronal promoter *elavl3* (*Tg(elavl3:CaMPARI(W391F+V398L))*⁵⁸). CaMPARI is a permanent photoconvertible calcium sensor that undergoes allosteric chromophore modulation from green to red in response to UV light, but only upon simultaneous binding of free intracellular calcium.⁵⁸ To achieve neuron-specific expression of a transgene of interest, we used a neuron-driven Gal4 line, *Tg(elavl3:Gal4-VP16)*.⁵⁹ Likewise, to achieve macrophage-specific expression of a transgene, we used a macrophage-driven Gal4, *Tg(mpeg1:Gal4FF)*.^{60,61} To visualize neurons and macrophages simultaneously, we used a photoconvertible pan-neuronal transgenic line in which the neurons express a photoconvertible protein, Kaede, that converts from green to red in response to blue light, *Tg(HuC:Kaede)*.⁶⁰ To visualize macrophages in the red channel as a control experiment for the optogenetic stimulation study, we used a transgenic line with UAS-driven nitroreductase fused to mCherry, *Tg(UAS:nfsB-mCherry)*⁶¹ and crossed these fish with the macrophage-Gal4 line. To determine whether PFOS-induced microglial dysfunction during early larval development influenced neuronal excitation and behavior, we used the embryonic macrophage mutant line targeting the gene *irf8* (TALE-NT 2.0; frameshift mutation of the st96 allele).⁶² *Irf8* mutants lack all embryonic-derived macrophage populations, including microglia.⁶²

PFOS and PFOA Exposure

PFOS (Sigma-Aldrich, Cat. No. A-5040) and PFOA (Sigma-Aldrich, Cat. No. 171468) were prepared by dissolving the powdered compounds in 100% dimethyl sulfoxide (DMSO). PFOS and PFOA stock concentrations were verified using liquid chromatography high-resolution mass spectrometry (LC-HRMS; certified reference standards and internal standards were purchased from Wellington). Upon verification of the stock concentration, we found that the PFOS solution contained the following impurities: 4,409.49 ng/L of perfluoroheptane sulfonic acid (PFHpS), 4,588.56 ng/L of perfluorohexanesulfonic acid (PFHxS), and 7,493.40 ng/L of perfluorononanesulfonic acid (PFNS). PFOS and PFOA stock solutions were diluted by a factor of 5,000 \times in a mixture of 1:1 methanol:water and 2 mM ammonium acetate to accommodate the detection range of the LC-HRMS. LC/MS-grade water and methanol were purchased from Honeywell. Ammonium acetate solution (5 M) was purchased from Millipore Sigma.

Timed spawns of relevant transgenic zebrafish crosses were performed for 1 h. Embryos were collected and screened for embryo quality at 4 hpf. Healthy embryos were placed in 24-well plates at a density of three embryos per well. Prior to treatment, PFAS compounds were diluted in egg water (60-mg/L Instant Ocean Sea Salts; Aquarium Systems) to the final concentration of interest. Egg water containing 0.1% DMSO was used as the vehicle control. Embryos were dosed with 2 mL of diluted PFOS solution or vehicle control per well at 4 hpf. The 24-well plates were sealed with parafilm to limit evaporative loss and placed in an incubator (28.5 \pm 1°C). Embryos were decolonized at 24 hpf and statically exposed until the experimental time point of interest. PFOS body burden was assessed at 48 hpf and 72 hpf, as described in the section “Targeted Analysis of PFOS Using LC-HRMS” below.

We selected a range of PFOS concentrations based on previously published developmental toxicology research that provided important information regarding mortality and gross morphological changes in response to exposure in larval zebrafish at similar time points.^{63,64} The survival rate following exposure to the three highest concentrations of PFOS used in the study (14 μ M PFOS, 28 μ M PFOS, and 56 μ M PFOS) was determined between 24 hpf [1 d postfertilization (dpf)] and 120 hpf (5 dpf). At 120 hpf, there was no significant difference in larval survival in the 14 μ M PFOS-exposed group. However, significant reductions in survival rates were first detected at 96 hpf in the 28 μ M and 56 μ M PFOS-exposed groups (Table S1). As such, larvae exposed to 7 μ M and 14 μ M PFOS were assessed until 5 dpf, whereas larvae exposed to 28 μ M or 56 μ M PFOS were assessed until 3 dpf.

Brain Injury Model

At 3 dpf, larval zebrafish were anesthetized in 0.02% Tricaine-S solution (Syndel, MS-222) and restrained dorsal side up in 2% agarose (Fisher Scientific, Cat. No. BP160-100). The larvae were injured anteriorly at the right telencephalon with a 9- μ m OD pulled-glass capillary needle. This method was an adaptation for larval fish.⁶⁵ For time-lapse imaging, larvae were immediately mounted dorsally on a 35-mm glass-bottom microwell dish (MatTek, Part No. P35G-1.5-14-C) in 2% low-melting agarose (Fisher Scientific, Cat. No. BP160-100) surrounded by egg water. Multi-slice projection images of the forebrain (FB) and optic tectum (OT) at various time points post-injury, as well as time-lapse videos composed of 10-min imaging intervals, were captured using a Zeiss LSM 880 confocal microscope at 20 \times magnification. Area of microglia response was measured using Zen Blue (Zeiss).

Microglial Cell Quantification

Adult transgenic zebrafish expressing *Tg(HuC:Kaede)* and *Tg(mpeg1:EGFP)* were crossed to generate *Tg(HuC:Kaede; mpeg1:EGFP)* fish, which had pan-neuronal expression of the photoconvertible protein Kaede, as well as green macrophages. Embryos were exposed to PFOS, as described above. At 3 dpf, larvae were fixed in 4% paraformaldehyde (PFA; Sigma-Aldrich, Cat. No. P6148) for 18–24 h at 4°C. Post-fixation, larvae were washed three times in phosphate buffered solution + 0.6% Triton-X 100 (PBS-T) (Sigma-Aldrich, Cat. No. X100). PBS-T was removed and VECTASHIELD Mounting Media (Vector Labs, Cat. No. H-1000) was added to the samples. The samples were incubated for 5 min at room temperature and then were gently mixed and held at –20°C until imaging. The larvae were removed from VECTASHIELD and mounted in 2% low-melting agarose (Fisher Scientific, Cat. No. BP160-100) in 35-mm glass-bottom microwell dishes (MatTek, Part No. P35G-1.5-14-C). Prior to image acquisition, the Kaede fluorophore was photoconverted from green to red fluorescence using 405-nm light (about 1-min exposure) on the Zeiss LSM 880 confocal microscope. Microglia were defined as macrophages (mpeg1⁺ cells) among and in contact with differentiated neurons (HuC⁺ cells) in the FB, OT, and hindbrain (HB). The entirety of the zebrafish brain was imaged at 20 \times magnification (2 tile panels with 10% overlap). Microglia were counted by panning through confocal z-stacks using FIJI/ImageJ.⁶⁶ Immune cells in contact with HuC⁺ differentiated neurons were counted as parenchymal cells (i.e., microglia). Surface cells in contact with differentiated neurons that failed to extend into the parenchyma were defined as nonparenchymal cells (i.e., macrophages). Location and proximity of mpeg1⁺ cells were confirmed using z-stack orthogonal views.

Microglial Morphology Quantification following PFOS Exposure

Microglial morphology was performed on high-resolution confocal micrographs of the OT in fixed transgenic zebrafish larvae expressing either *Tg(mpeg1:EGFP)*, *Tg(mpeg1:Gal4FF;UAS:eNpHR3.0-mCherry)*, or *Tg(mpeg1:Gal4FF;UAS:nfsb-mCherry)*. Individual microglia were isolated based on their specific z-stack range, to prevent analysis of overlapping cells, using FIJI/ImageJ.⁶⁶ Z-slices were also processed to rescale intensity (compensating for loss of intensity in deeper tissue) and modestly smoothed using Gaussian blur with a sigma radius of 1 to better define cellular extensions and reduce signal noise. Each cell was individually outlined, and morphological parameters measured with CellProfiler software (version 3.1.9) or FIJI/ImageJ.⁶⁶ Area, perimeter, and cell shape (perimeter-to-area ratio) were quantified.

Quantitative Real-Time Polymerase Chain Reaction

Larval zebrafish heads were collected at 3 dpf. To collect the heads, the larvae were placed on ice for 4 min to immobilize swim activity and prevent pain or distress during collection.⁶⁷ The heads were removed by cutting at the base of the HB at a 45° angle, limiting collection of the heart and pericardium. Heads were pooled ($n = 10$) and flash frozen in liquid nitrogen. Four independent experimental replicates were collected per treatment group. RNA isolation and purification was carried out using the Rneasy Plus Kit (QIAGEN). Complementary DNA (cDNA) synthesis was achieved using the SuperScript IV Reverse Transcriptase First-Strand Synthesis System kit (Invitrogen, Cat. No. 18091050). Quantitative real-time polymerase chain reaction (qRT-PCR) for the genes of interest was performed with 7.5 ng/ μ L of cDNA using the ViiA7 RT-PCR System (Applied Biosystems). Gene targets were detected by using either predesigned TaqMan probes (Thermo Fisher Scientific) or

custom primers with Power Track SYBR Green Master Mix (Thermo Fisher, Cat. No. A46012). See list of probes and primers for qRT-PCR and genotyping in Table S2.

Genotyping *irf8* Mutants

irf8^{st96/st96} were generated by Shiau et al. via TALEN-targeting.⁶² After swim behavior testing or CaMPARI imaging, whole larvae were placed directly in 50 μ L of DNA lysis buffer [10 mM Tris pH 8.4 (Fisher, Cat. No. BP152-500), 50 mM potassium chloride (Sigma, Cat. No. P9333), 1.5 mM magnesium chloride (MgCl₂; Sigma, Cat. No. M0250), 0.30% Tween-20 (Fisher, Cat. No. BP337), 0.30% Igepal/NP-40 (Sigma, Cat. No. 56741)] to be used for genotyping. The larvae were incubated in DNA lysis buffer for 20 min at 94°C, cooled to 55°C, then 5 μ L of 10-mg/mL proteinase K (Millipore Sigma, Cat. No. 70663-4) was added. All temperature-specific reactions were carried out in the ProFlex PCR System (Applied Biosystems). Samples were incubated for 1 h at 55°C, followed by 20 min at 94°C and then held at 4°C until the PCR reaction. The PCR reaction was performed with 2 μ L of DNA and 18 μ L of master mix [deionized water (diH₂O), 10 \times Taq Buffer (Thermo Scientific, Cat. No. EP0404), 2.5 mM deoxynucleotide triphosphates (dNTP; Thermo Scientific, Cat. No. R1121), 25 mM MgCl₂ (Thermo Scientific, Cat. No. AB0359), 10 μ M forward primer (IDT), 10 μ M reverse primer (IDT), DMSO (Millipore Sigma, Cat. No. D8418), and Taq DNA polymerase (Thermo Scientific, Cat. No. EP0404)]. The PCR reaction conditions were as follows: 1 min at 95°C; 35 cycles of 30 s at 95°C, 45 s at 68°C, and 30 s at 72°C; then 7 min at 72°C; and hold at 4°C. The *irf8* exon 1 fragment was amplified using primers listed in Table S2. Given that this *irf8* mutant has a frameshift mutation at an *Ava*I site, the PCR product was used for restriction digest with *Ava*I (New England BioLabs, Cat. No. R0152L) to identify the presence of the mutation. For the restriction digest reaction, 10 μ L of PCR product and 10 μ L of digest master mix (diH₂O; rCutSmart Buffer, and *Ava*I) were combined and run on the thermocycler for 20 min at 37°C and then cooled to 4°C. The digest reaction product was run in a 2% agarose gel containing RedSafe nucleic acid staining solution (Bulldog Bio Inc, Cat. No. 21141). The gel results were visualized using the Bio-Rad Gel Doc XR+.

Acridine Orange Staining

Cell death was determined using the vital dye acridine orange (AO) in live zebrafish embryos. AO is a cell-permeable stain that selectively intercalates uncoiled nucleic acid present in apoptotic cells.⁶⁸ Zebrafish embryos were injured at 3 dpf and placed in 5- μ g/mL AO (ThermoFisher, Cat. No. A1301) diluted in egg water for 20 min. The zebrafish were then washed in egg water for 15 min, refreshing the solution every 5 min. Live zebrafish were mounted in 2% agarose and immediately imaged on a Zeiss LSM 880 confocal microscope. For 1 h post-injury (hpi) analysis, staining took place from 40 min to 1 hpi. For 4 hpi analysis, staining took place from 3 h and 40 min to 4 hpi.

CaMPARI Photoconversion and Image Acquisition

Tg[elavl3:CaMPARI(W391F+V398L)]^{ir9} embryos were screened and the brightest (highest expressing) were selected for toxicant exposure and subsequent photoconversion. At either 3 dpf or 5 dpf, CaMPARI-positive larvae were individually placed into a modified 1-well dish (15-mm diameter) containing PFOS or 0.1% DMSO. The dish was placed onto a constructed pedestal within a DanioVision Observation Chamber (Noldus) adapted with optogenetics components (Prizmatix). Use of the pedestal decreased working distance from the LED light source to the free-swimming larva, concordantly increasing light intensity. Cells expressing

CaMPARI with high calcium content will photoconvert (green to red) in the presence of 405-nm light. Photoconversion was performed by exposing the zebrafish to 405-nm (135 mW/cm²) wavelength light for 1 min. Live zebrafish larvae were then anesthetized in 0.02% Tricaine-S (Syndel, MS-222) and mounted in 2% low-melting agarose in 35-mm glass-bottom microwell dishes. Confocal z-stacks were acquired on a Zeiss LSM 880 confocal microscope and maximum intensity projections generated in Zen Black (Zeiss) representing a global snapshot of neural activity. Image parameters were set during acquisition of the first image and maintained for the duration of each experiment.

CaMPARI Analyses (Red/Green Ratio Calculations)

CaMPARI photoconversion from green to red during exposure to 405-nm wavelength light was used to determine neuronal calcium levels following PFOS exposure at 3 dpf or 5 dpf. To assess the level of photoconversion, maximum intensity projections were imported into FIJI/ImageJ.⁶⁶ Brain regions of interest—including FB, habenula (H), OT, cerebellum (Ce), HB, and whole brain (WB)—were manually selected, and the integrated density of red and green was measured. Measurements were blank-corrected by selecting three separate background regions of each image (Equation 1). The ratios of corrected integrated density were then used to determine the red/green (R/G) ratio for each respective image (Equation 2). R/G ratios were then normalized to the average control R/G ratio within a particular experiment (Equation 3).

$$C = d - \left(\frac{\Sigma(b1 + b2 + b3)}{3} \right), \quad (1)$$

where *b* is the background integrated density, and *d* is the integrated density of region of interest.

$$R = C_{Red} / C_{Green}, \quad (2)$$

$$\text{Normalized R/G Ratio} = R / \bar{X}, \quad (3)$$

where \bar{X} is mean of control R/G ratios (for each experimental day).

Pentylentetrazol Exposure

For validation of CaMPARI functionality, 3 dpf *Tg[elavl3:CaMPARI(W391F+V398L)]^{ir9}* larvae were exposed to 10 mM pentylentetrazol (PTZ) for 10 min. PTZ was washed out three times with egg water immediately followed by CaMPARI photoconversion, as described above. For assessment of microglia response to injury following PTZ exposure, the larvae were exposed to control solution, 28 μ M PFOS, or 5 mM PTZ at 3 dpf. The larvae were injured in the right telencephalon, as described above, and placed back in their original dosing solutions for 4 h. At 4 hpi, larvae were mounted in 2% agarose in a 35-mm glass-bottom imaging dish and multi-slice projection images of the FB and OT were captured using a Zeiss LSM 880 confocal microscope at 20 \times magnification. The area of microglia response was measured using Zen Blue (Zeiss).

Light/Dark Behavioral Assay

Behavioral assessments were performed in 24-well plates (ThermoFisher, Cat. No. 144530) using a DanioVision Observation Chamber with EthoVision XT live-tracking software (Noldus). Larval zebrafish were exposed to either the control solution or 7 μ M, 14 μ M, or 28 μ M PFOS at 4 hpf, as described above. Approximately 18–24 hours prior to behavioral assessment, the larvae were transferred into individual wells of the same dosing solution. All dosing solutions were prepared and plated on the same day as the initial

larval exposure to maintain chronic exposure conditions, rather than introducing the larvae to a fresh dosing solution. All light/dark behavioral assays were performed between 0800 and 0000 hours to prevent behavioral changes attributable to circadian differences. Briefly, the zebrafish were placed into the DanioVision Observation Chamber and acclimated during a 15-min dark cycle, followed by a 5-min light cycle (Light 1), a 5-min dark cycle (Dark 1), another 5-min light cycle (Light 2), and completed with a 15-min dark cycle (Dark 2). Behavioral experiments lasted a total of 45 min.

Total distance moved (in millimeters) during light/dark cycles was quantified using the EthoVision XT software as a measure for hyperactivity. Anxiety-like behavior following PFOS exposure was assessed by monitoring larval well location (center vs. edge) over the course of the assay. Defined center and edge regions each constituted 50% of total well area. Edge vs. center preference was quantified using EthoVision XT. Center-avoidance data was normalized relative to controls for each experimental replicate.

Optogenetic Manipulation in Noldus Behavioral Unit

To stimulate the optogenetic channel halorhodopsin in the transgenic lines *Tg(elavl3:Gal4;UAS:eNpHR3.0-mCherry)* and *Tg(mpeg1:Gal4ff;UAS:eNpHR3.0-mCherry)*, screened larvae were placed in a DanioVision Observation Chamber (Noldus) outfitted with a 570-nm wavelength laser (Prizmatix). Halorhodopsin's peak excitation wavelength is 589 nm although, because its excitation spectrum is broad, halorhodopsin is also responsive to 570-nm light. Halorhodopsin⁺ neurons or microglia were stimulated with 570-nm light for 4 h then immediately imaged for cell morphology or injury response.

Targeted Analysis of PFOS Using LC-HRMS

Body burden was assessed at 48 hpf and 72 hpf to determine the level of uptake of PFOS in the larvae, as well as to determine the extent to which the detected PFAS impurities (PFNS, PFHpS, PFHxS) were present in the larvae. Body burden results are in Table S3. Certified PFOS, PFNS, PFHpS, and PFHxS and their respective isotope-labeled reference standards were purchased from Wellington Laboratories. LC/MS-grade water and methanol were purchased from Honeywell. Ammonium acetate solution (5 M) was purchased from Millipore Sigma.

Sample extraction. Three technical replicates of 10 larvae were pooled, flash frozen in liquid nitrogen, and stored in a -80°C freezer until extracted and defrosted at 20°C . The extraction was performed by adding 1 mL methanol to the embryo centrifuge tube, sonicating the samples for 90 min, vortexing to mix for 1 min, followed by refrigeration for 3 h at 20°C and then centrifugation at 3,000 rpm for 10 min. The extract (50 μL) was added to an analysis vial with 10 μL of labeled PFOS internal standard and 440 μL of 1:1 methanol:water and 2 mM ammonium acetate.

Targeted PFOS analysis was performed using a Thermo LC Orbitrap Q Exactive HF-X MS equipped with a Thermo Vanquish ultra-high-performance LC (UHPLC) system. Samples were injected in triplicate in 20- μL volumes. Components were separated using two mobile phases (A: 2 mM aqueous ammonium acetate; B: 2 mM ammonium acetate in methanol) and a Thermo Hypersil Gold Vanquish C18 column (50 mm \times 2.1 mm \times 1.9 μm) at 60°C . PFOS was eluted from the column at a constant flow rate of 0.4 mL/min, using a mobile phase gradient as follows: equilibration with 10% B for 1 min, followed by a gradient ramp from 10% B to 95% B over 4 min and held for 2 min, and back to 10% B over 1 min and held for 2 min (total run time 9 min, and data were collected from minute 0.6 to minute 8.5). Ionization was performed in negative mode with a 1.0 m/z ionization window, 40 sheath gas flow rate (unitless), 10 auxiliary gas flow rate (unitless), 2 sweep gas

flow rate (unitless), 2.7-kV spray voltage, 310°C capillary temperature, 34 funnel radio frequency (RF) level (unitless), and 320°C auxiliary gas heater temperature. Full scan data-dependent (dd)-MS² mode (70 normalized collision energy (NCE), 120,000 resolution for MS¹, 3×10^6 automatic gain control, and 100-ms maximum dwell time) was used with a PFOS inclusion list. MS² fragmentation was performed in the higher-energy collisional dissociation (HCD) collision cell filled with nitrogen gas (produced by a Peak Scientific Nitrogen Generator, Genius NM32LA) and a resolution of 15,000, 2×10^5 , and maximum dwell time of 400 ms.

Four ions were monitored for PFOS, including 498.9302 m/z (quantifying), 79.9573 m/z (confirming), 98.9556 m/z (confirming), and 82.9607 m/z (confirming). The retention time of PFOS was 5.18 min. TraceFinder (version 5.0 General; Thermo Fisher Scientific) was used for quantification with an external 7-point calibration curve. Limits of detection (LODs) were determined by injecting a calibration standard seven times and using Equation 4:

$$LOD = (3 \times s)/m, \quad (4)$$

where s is the sample standard deviation, and m is the calibration curve slope. The resulting PFOS LOD was 33.87 ppt.

Untargeted MWAS

High-resolution metabolomics. The sample extracts were reanalyzed using LC-HRMS to collect untargeted metabolomics data. Normal-phase (Thermo Synchronis hydrophilic interaction LC column, 50 mm \times 2.1 mm \times 3 μm at 25°C) and reverse phase (Thermo Hypersil Gold Vanquish C18 column, 50 mm \times 2.1 mm \times 1.9 μm at 60°C) chromatography were performed with triplicate 10- μL injections onto the LC-HRMS system, as described above. For normal-phase, metabolites were eluted from the column using a 0.2-mL/min flow rate and two mobile phases (A: 2 mM ammonium acetate in acetonitrile; B: 2 mM aqueous ammonium acetate). The solvent gradient was as follows: equilibrate with 10% B for 1 min, increase to 65% B until 10 min, hold at 65% B until 13 min, decrease to 10% B until 14 min, and hold at 10% B until 15 min. For reverse phase, metabolites were eluted from the column using a constant of a 0.5-mL/min flow rate and two mobile phases (C: 2 mM aqueous ammonium acetate; D: 2 mM ammonium acetate in acetonitrile). The reverse phase solvent gradient was as follows: equilibration with 2.5% C until 1 min, increase to 100% C until 12 min, hold at 100% C until 14 min, and decrease to 2.5% C until 15 min, and hold at 2.5% C until 16.5 min. Electrospray ionization was positive mode for normal-phase and negative mode for reverse phase LC. Full scan dd-MS² data was collected using the same settings as described in the targeted PFOS section with the following exceptions: 2.7-kV spray voltage and 35 funnel RF level (unitless).

Metabolomics data analysis. Data files were converted from *.raw files to *.cdf files using Xcalibur file Converter. Feature tables with paired mass-to-charge ratio and retention time values were created in R (version 4.2.0; R Development Core Team) using packages apLCMS⁶⁹ and xMSanalyzer.⁷⁰ Association of log₂-normalized metabolite features with PFOS exposure was assessed using a t -test ($p < 0.05$) in comparison with the control samples. Significant metabolites (those having adjusted Benjamini-Hochberg p -values with a false discovery rate (FDR)⁷¹ $\leq 20\%$) were analyzed for pathway enrichment using MetaboAnalyst⁷² using the zebrafish mummichog-curated model, which includes the Kyoto Encyclopedia of Genes and Genomes (KEGG), BiGG (<http://bigg.ucsd.edu>), and Edinburgh maps.

Statistical Analyses and Reproducibility

Each experiment was carried out in at least three independent experimental replicates. An experimental replicate was considered

a cohort of zebrafish that were spawned on separate days and, when applicable, dosed with separate freshly prepared dosing solutions. Dosing groups for each experimental replicate were composed of siblings, such that sibling controls could be compared with dosed siblings. For each graph, data sets were tested for normality using a Shapiro–Wilk test and by plotting a QQ plot. If the data were normally distributed, parametric tests were performed, when applicable. If the data were not normally distributed, nonparametric tests were performed, when applicable. When comparing two independent groups, unpaired parametric *t*-tests with Welch's correction were performed if the data were normally distributed, or Mann Whitney *U*-tests (nonparametric) were performed if the data was not normally distributed. In cases where there were three or more groups with one independent variable and the data were normally distributed, a Welch analysis of variance (ANOVA) with post hoc Dunnett's T3 multiple comparisons test was performed. In cases where there were three or more groups with one independent variable and the data were not normally distributed, a Kruskal–Wallis test (nonparametric ANOVA) with Dunn's test for multiple comparisons was performed. In cases where there were three or more groups with two independent variables and the mean of each group was compared with the mean of every other group, a two-way ANOVA with a post hoc Tukey multiple comparisons test was performed. In cases where there were three or more groups with two independent variables and the mean of two selected groups were selected for comparison, a two-way ANOVA with a post hoc Sidak multiple comparisons test was performed. All statistical analyses were performed using GraphPad Prism (version 9; Dotmatics).

Data Availability

All data is available in the main text and Supplemental Materials. All targeted and untargeted metabolomics files from this study are available at the NIH Common Fund's National Metabolomics Data Repository (NMDR) website, the Metabolomics Workbench,⁷³ <https://www.metabolomicsworkbench.org>, where it has been assigned study ID ST002768. The data can be accessed directly via its project DOI: <http://dx.doi.org/10.21228/M8QX5M>. This work was supported by NIH grant U2C-DK119886.

Results

Microglial Morphology and Response to Brain Injury following Chronic PFOS Exposure

Whether PFOS affects microglia development and function *in vivo* is not yet known. Given the critical developmental and modulatory roles of microglia in the CNS, we sought to determine whether embryonic exposure to PFOS had a direct effect on microglia colonization of the developing brain. Transgenic zebrafish embryos with macrophage-specific green fluorescent protein (GFP) expression under the *mpeg1* promoter [*Tg(mpeg1:EGFP)*]⁵⁵ were chronically exposed to either a control solution (0.1% DMSO) or 28 μ M PFOS from 4 hpf until 3 dpf (Figure 1A). Using LC-HRMS, we validated our exposure solutions and determined that 28 μ M PFOS resulted in a total body burden of 70.46 ± 2.72 ng/embryo at 3 dpf (Table S3). Next, we examined microglial number and morphology at 3 dpf, a time point at which no significant differences in mortality were observed across the tested concentration range (Table S1). Nonparenchymal, parenchymal, and total microglia number was not different at 3 dpf between the control and 28 μ M PFOS-exposed larvae (Figure S1A–C). Although microglia number was similar, cell morphology was significantly different. PFOS-exposed microglia acquired a less ramified and more amoeboid cell shape (Figure 1D–E'' vs. 1I–J'').

This corresponded to a significantly smaller cell area (Figure 1N), cell perimeter (Figure 1O) and the acquisition of a more circular cell shape as calculated by a decrease in the perimeter-to-area ratio (Figure 1P). Relative mRNA transcripts for the gene *p2ry12*, a G-protein coupled receptor for ATP directly involved in microglia activation and migration behavior,^{74–76} were also significantly up-regulated in the brains of PFOS-exposed larvae (Figure 1Q), further supporting that PFOS exposure was affecting microglia state.

To determine whether the phenotypic and transcriptional differences were accompanied by functional differences, we tested whether pollutant-induced microglia activation affected the ability of microglia to respond to minor brain injury using an established zebrafish injury model.^{77,78} At 3 dpf, larvae were injured at the right hemisphere of the telencephalon using a pulled-glass needle (OD 9 μ m; Figure 1B) and microglia recruitment to the injury site was monitored for the first 4.5 h post-injury (hpi; Figure 1C). PFOS-exposed larvae had significantly more microglia recruit to the injury site in the first 4.5 hpi compared with sibling controls (Figure 1R; Supplemental Videos 1 vs. 2). In addition, the area of microglial response in exposed larvae was significantly expanded at 4 hpi (Figure 1G vs. 1L; Figure 1S), which persisted up to 12 hpi (Figure 1H vs. 1M; Figure 1T). A major function of microglia following brain injury is the removal of damaged cells and cellular debris to prevent excessive inflammation, which is deleterious to brain health.⁷⁹ Using the nucleic acid stain AO in live larvae, we asked whether an increased incidence of cell death was driving the microglia response to injury in pollutant-exposed larvae; however, PFOS exposure did not result in more cell death in the WB nor at the injury site at 1 or 4 hpi (Figure S1D–H). Moreover, relative mRNA expression of the proinflammatory cytokines *il1 β* , *tnf α* , and *il6* were not different in larval brains following exposure compared with those in the control group (Figure S1I).

Microglia Morphology and Response to Brain Injury following Optogenetic Reversal of Microglia Activation State in PFOS-Exposed Larvae

To determine the extent to which the microglia state contributed to the heightened microglial response to injury, we next asked whether PFOS-induced changes in microglia state could be reversed *in vivo*, as well as whether this reversal of state was sufficient to normalize the injury response. Given that the homeostatic microglia membrane potential is largely maintained by chloride channel currents,⁸⁰ we used transgenic zebrafish expressing the light-gated chloride pump halorhodopsin (eNpHR3.0) specifically in microglia [*Tg(mpeg1:Gal4FF;UAS:eNpHR3.0-mCherry)*] (Figure 2A). Larvae with halorhodopsin⁺ microglia were exposed to 28 μ M PFOS, injured at 3 dpf, and exposed to 570-nm light for 4 h (Figure 2B,C) to induce the halorhodopsin construct specifically in *mpeg1*⁺ cells. We confirmed the PFOS-induced changes in microglial morphology in unstimulated PFOS-exposed larvae (Figure 2D–E''), consistent with Figure 1, and compared the microglia morphology of these unstimulated larvae to PFOS-exposed larvae stimulated with 570-nm light. Halorhodopsin stimulation of PFOS-exposed microglia produced a significantly more ramified morphology (Figure 2H–I''). In addition, although the microglia area was not different between stimulated and unstimulated fish (Figure 2L), cell perimeter (Figure 2M) and perimeter-to-area ratio (Figure 2N) were significantly greater in the stimulated group, supporting the transition from an amoeboid to a ramified state. We also confirmed that 570-nm stimulation alone had no impact on microglia morphology by stimulating and assessing microglia from PFOS-exposed larvae lacking halorhodopsin expression, *Tg(mpeg1:Gal4FF;UAS:nfsb-mCherry)* (Figure S2). We next tested whether optogenetic modulation of microglia state was sufficient to rescue their responses to

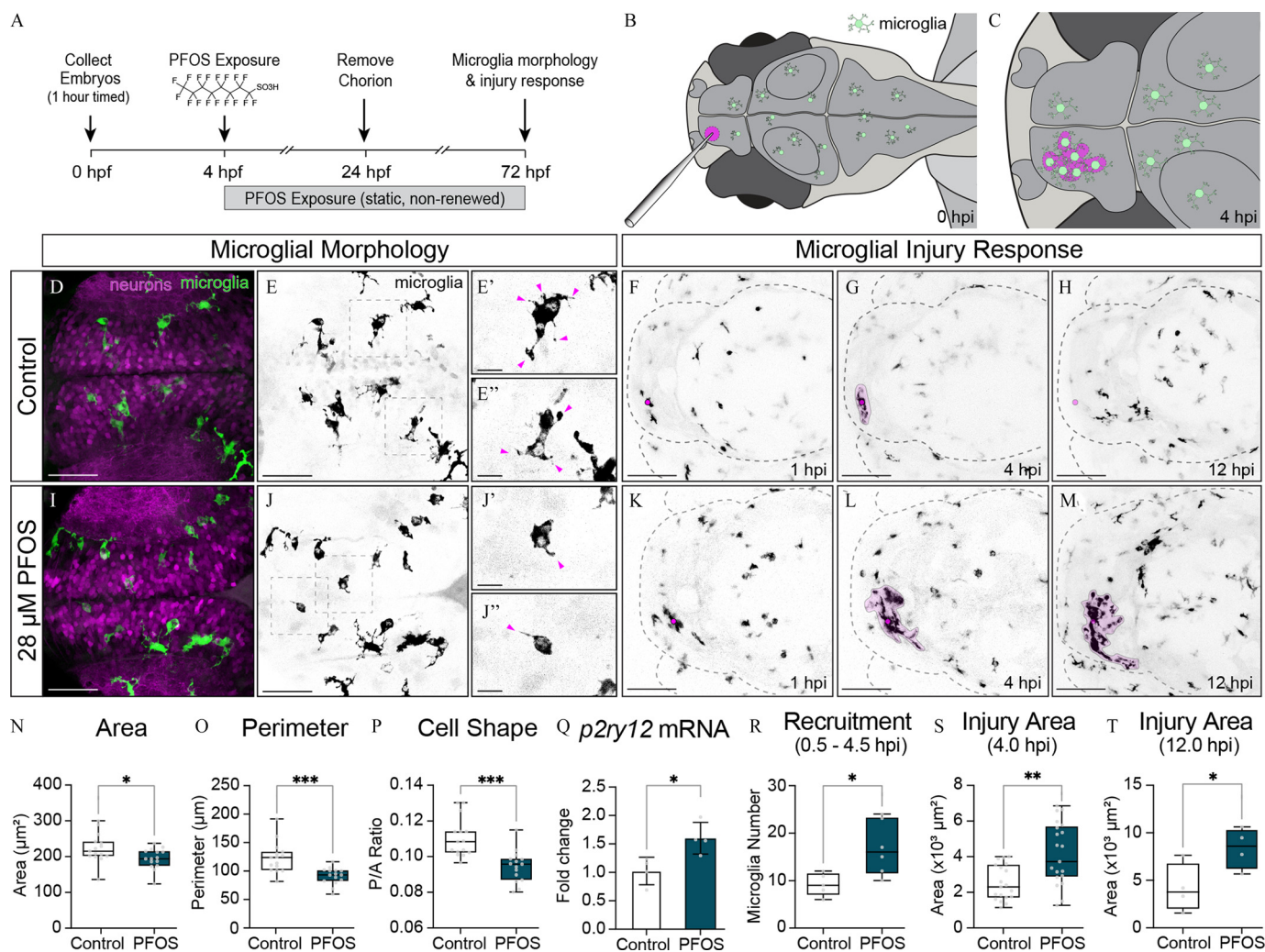


Figure 1. Microglia morphology and response to minor brain injury in 3-dpf larvae exposed to 28 μM PFOS. (A) Exposure paradigm: zebrafish embryos from *Tg(mpeg1:EGFP)* adults were collected after a 1-h timed spawn. At 4 hpf, embryos were dosed with 0.1% DMSO (Control) or 28 μM PFOS. Treatment solutions were static and not renewed. Embryos were dechorionated at 24 hpf, and imaging and injury experiments were conducted at 3 dpf. (B) Schematic of larval brain injury: a pulled-glass needle (OD 9 μm) was used to puncture the right telencephalon of larval zebrafish. (C) Hypothetical schematic of microglia response 4 h post-injury (hpi). (D) Confocal micrographs of 3-dpf control-treated larvae with fluorescently labeled neurons and microglia. (E) Isolated fluorescently labeled microglia from (D). (E'–E'') 3 \times magnified microglia from boxes in (E). Magenta arrows point to projections emanating from the microglia cell bodies. (F) Dorsal view of a representative 3-dpf control-treated larval brain at 1 hpi. Injury site marked with magenta dot. (G) Dorsal view of a representative 3-dpf control-treated larval brain at 4 hpi. (H) Dorsal view of a representative 3-dpf control-treated larval brain at 12 hpi. (I) Confocal micrographs of 3-dpf 28 μM PFOS-treated larvae with fluorescently labeled neurons and microglia. (J) Micrographs from (I) isolating just the fluorescently labeled microglia. (J'–J'') 3 \times magnified microglia from boxes in (J). Magenta arrows point to projections emanating from the microglia cell bodies. (K) Dorsal view of a representative 3-dpf 28 μM PFOS-treated larval brain at 1 hpi. Injury site marked with magenta dot. (L) Dorsal view of a representative 3-dpf 28 μM PFOS-treated larval brain at 4 hpi. (M) Dorsal view of a representative 3-dpf 28 μM PFOS-treated larval brain at 12 hpi. (N) Quantification of microglia cell area. (O) Quantification of microglia cell perimeter. (P) Perimeter-to-area ratio of control-treated and PFOS-treated microglia. $n = 15$ fish per group; 3–18 cells counted per fish. (Q) qRT-PCR results assessing the relative expression of the microglia activation gene, *p2ry12*, in isolated heads of control- and PFOS-treated 3-dpf larvae. $n = 4$ samples of 10 pooled heads. (R) Number of microglia recruited to the injury site between 0.5 and 4.5 hpi. $n = 5$ –6 per group. (S) Quantification of the area of microglia response around the injury site at 4 hpi, as shown as the magenta overlays in (G) and (I). $n = 19$ –20 fish per group. (T) Quantification of the area of microglia response around the injury site at 12 hpi. $n = 4$ fish per group. Confocal micrographs at 40 \times magnification (D–E'' and I–J'') or 20 \times magnification (F–H; K–M). Error bars represent standard deviation. Box plot limits represent 25th to 75th percentile, with the midline representing the median. * $p < 0.05$; ** $p < 0.01$; *** $p < 0.001$. See Excel Table S1 for additional statistical details. Note: DMSO, dimethyl sulfoxide; dpf, days post fertilization; hpi, hours postfertilization; PFOS, perfluorooctane sulfonate.

brain injury. Indeed, although unstimulated larvae had exacerbated microglial responses to injury (Figure 2F vs. 2G), PFOS-exposed halorhodopsin⁺ microglia were significantly less responsive (Figure 2G vs. 2K; area of response quantified in Figure 2O).

Assessment of Global and Regional Neuronal Network Activity in PFOS-Exposed Larvae Using CaMPARI

Given that microglia are highly responsive to their microenvironments, microglia hyperresponsiveness in PFOS-exposed larvae may

be influenced by changes in neuronal communication. Although evidence suggests PFOS exposure can impact developing and adult brain health, the direct effects of exposure on neuronal network activity, WB metabolome, and neurotransmitter release are not well understood. To understand the effect of PFOS on global brain activity *in vivo*, we assessed neuronal calcium activity by driving the fluorescent calcium sensor CaMPARI under the pan-neuronal promoter *elavl3* (*Tg(elavl3:CaMPARI(W391F+V398L))^{fl9}*). CaMPARI is a permanent photoconvertible calcium sensor

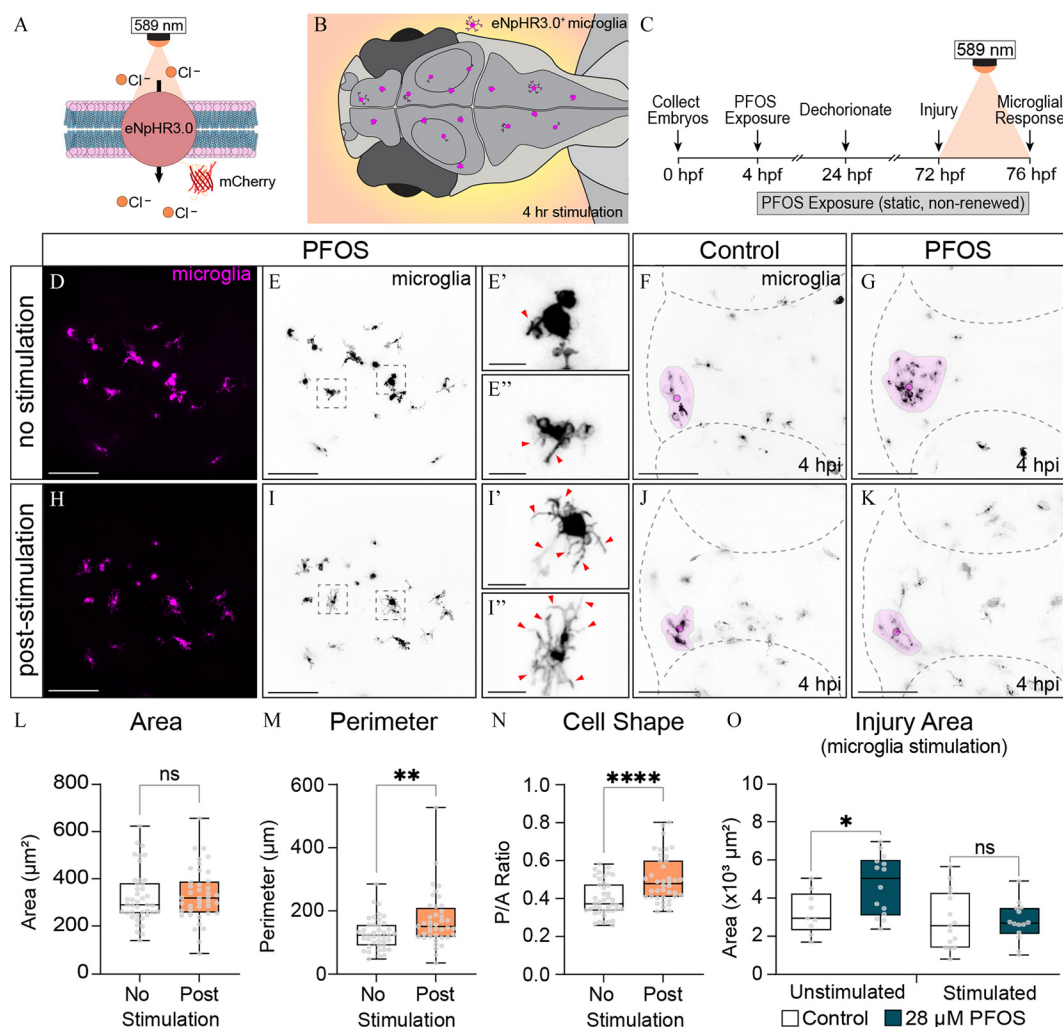


Figure 2. Optogenetic modulation of PFOS-exposed microglia. (A) Schematic of halorhodopsin: Optogenetic modulation of microglia electrical state is achieved via photostimulation of the light-gated chloride pump, halorhodopsin (eNpHR3.0). eNpHR3.0 is most responsive to 589-nm wavelength light. (B) eNpHR3.0 was driven under a pan-macrophage promoter [*Tg(mpeg1:GalFF;UAS:eNpHR3.0-mCherry)*] to achieve optogenetic control of microglia in zebrafish larvae. (C) Experimental paradigm: At 72 hpf, injured or uninjured zebrafish were stimulated for 4 h with 589-nm light in the enclosed Noldus DanioVision Behavior Unit. (D) Confocal micrograph of 3-dpf zebrafish brain exposed to 28 μM PFOS. Magenta cells are unstimulated halorhodopsin⁺ microglia. (E) Pseudocolored (D) in black and white. (E'–E'') 3 \times magnification of microglia from boxes in (E). Arrows point to projections emanating from the microglia cell bodies. (F) Dorsal view of a representative 3-dpf control-treated larval brain at 4 hpi without stimulation. Injury site marked with magenta dot and area of responding microglia shaded in magenta. (G) Dorsal view of a representative 3-dpf 28 μM PFOS-treated larval brain at 4 hpi without stimulation. (H) Confocal micrograph of 3-dpf 28 μM PFOS-treated larval brain following stimulation with 589-nm light. Magenta cells are stimulated halorhodopsin⁺ microglia. (I) Pseudocolored (H) in black and white. (I'–I'') 3 \times magnification of microglia from boxes in (I). Arrows point to projections emanating from the microglia cell bodies. (J) Dorsal view of a representative 3-dpf control-treated larval brain at 4 hpi following 589-nm light stimulation. (K) Dorsal view of a representative 3-dpf 28 μM PFOS-treated larval brain at 4 hpi following 589-nm light stimulation. (L) Quantification of microglia cell area of 3-dpf 28 μM PFOS-treated larvae with and without light stimulation. (M) Quantification of microglia cell perimeter of 3-dpf 28 μM PFOS-treated larvae with and without light stimulation. $n = 40$ – 42 cells per group from three independent experiments. (N) Perimeter-to-area ratio of individual microglia of 3-dpf 28 μM PFOS-treated larvae with and without light stimulation. $n = 40$ – 42 cells per group from three independent experiments. (O) Quantification of the area of microglia response around the injury site at 4 hpi. $n = 9$ – 15 fish per group. Confocal micrographs at $40\times$ magnification (D–E'' and H–I'') or $20\times$ magnification (F,G,J,K). * $p < 0.05$; ** $p < 0.01$; **** $p < 0.0001$. Error bars represent standard deviation. Box plot limits represent 25th to 75th percentile, with the midline representing the median. See Excel Table S1 for additional statistical details. Note: dpf, days post fertilization; hpi, hours postfertilization; ns, not significant; PFOS, perfluorooctane sulfonate.

that undergoes allosteric chromophore modulation from green to red in response to UV light, but only upon simultaneous binding of free intracellular calcium.⁵⁸ Therefore, inactive neurons at the time of photoconversion are green, whereas active neurons convert to red (Figure 3A–D). In this study, free-swimming larvae were subjected to 135 mW/cm^2 of 405-nm light for 1 min inside our Noldus behavioral unit (Figure S3A–D). We validated our CaMPARI photoconversion, imaging, and analysis pipeline by exposing larvae to PTZ, a gamma-aminobutyric acid subtype A (GABAA) receptor antagonist known to cause neuronal hyperactivity and seizures in zebrafish⁸¹ (Figure S3E–H vs. Figure 3E'–H').

Indeed, fish exposed to 10 mM PTZ exhibited significantly higher ratiometric expression of neuronal intracellular calcium in the OT (+22.2%) and 16.7% higher expression in the WB (Figure S3J). To determine whether PFOS exposure affected brain activity, we applied this validated pipeline to 3-dpf larvae exposed to 28 μM PFOS, the same concentration used for the injury model. Exposed fish had notably heightened neuronal activity in the FB (+11.4%), OT (+14.1%), Ce (+17.9%), HB (+14.6%), and WB collectively (+15.7%) compared with control fish (Figure 3G,I). We also examined whether lower concentrations of PFOS were able to induce differences in neuronal activity. Although there were no significant

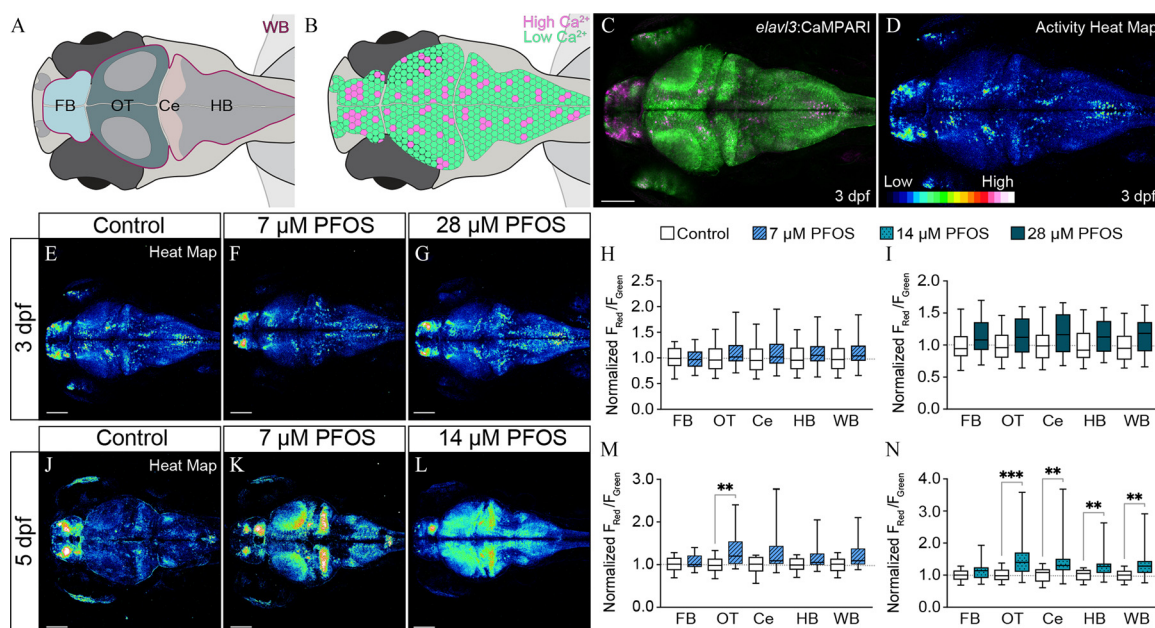


Figure 3. Analysis of regional and global neuronal network activity following chronic exposure to PFOS. (A) Illustrative representation of a larval zebrafish brain with anatomical regions outlined: forebrain (FB), optic tectum (OT), cerebellum (Ce), hindbrain (HB), and whole brain (WB). (B) Illustrative representation of neuron-driven CaMPARI: neurons with low intracellular calcium (low Ca^{2+}) remain green following 1-min exposure to 405-nm light, whereas neurons with high intracellular calcium (high Ca^{2+}) photoconvert to red. (C) Confocal micrograph of a 3-dpf larvae expressing neuron-specific CaMPARI [*Tg(elavl1:CaMPARI)*] following 1 min photoconversion. (D) Generated high-intensity look-up-table (LUT) heat map of the red, photoconverted channel in (C) depicting high-activity neurons. Low-to-high intracellular calcium is depicted by a blue–red–white spectrum. Confocal micrographs of active neurons at 3-dpf in (E) control and (F) 7 μM PFOS- and (G) 28 μM PFOS-exposed larvae following 1-min photoconversion with 405-nm light. Neuronal activity can be quantified by determining the ratio of fluorescent intensity in the red vs. green channels ($F_{\text{Red}}/F_{\text{Green}}$). (H) Quantification of the regional and global (i.e., WB) neuronal activity as normalized $F_{\text{Red}}/F_{\text{Green}}$ ratios of 3-dpf control or 7 μM PFOS-treated larvae. (I) Quantification of the regional and global neuronal activity of 3-dpf control or 28 μM PFOS-treated larvae. Confocal micrographs of active neurons at 5-dpf in (J) control and (K) 7 μM PFOS- and (L) 14 μM PFOS-exposed larvae following 1-min photoconversion with 405-nm light. (M) Quantification of the regional and global neuronal activity of 5-dpf control or 7 μM PFOS-treated larvae. (N) Quantification of the regional and global neuronal activity of 5-dpf control or 14 μM PFOS-treated larvae. Confocal micrographs at $10\times$ magnification. $n = 21\text{--}23$ fish per group. ** $p < 0.01$; *** $p < 0.001$. Error bars represent standard deviation. Box plot limits represent 25th to 75th percentile, with the midline representing the median. See Excel Table S1 for additional statistical details. Note: Ca^{2+} , calcium ion; CaMPARI, calcium-modulated photoactivatable ratiometric integrator; dpf, days postfertilization; PFOS, perfluorooctane sulfonate.

differences in network activity at 3 dpf following 7 μM PFOS exposure (Figure 3F,H), this group had notably and significantly heightened regional and global activity at 5 dpf (Figure 3K,M; FB, +7.1%; OT, +31.2%; Ce, +24.0%; HB, +15.7%; WB, +20.8%), as did the 14 μM PFOS-exposed group (Figure 3L,N; FB, +14.0%; OT, +52.6%; Ce, +51.8%; HB, +34.3%; WB, +39.6%). We also assessed gross brain morphology of PFOS-exposed larvae and found that although WB area was slightly smaller at 3 dpf in the 7 μM (−2.8%) and 14 μM (−2.7%) groups, brain area was not different at 5 dpf, suggesting that the effects of PFOS on morphology are nominal and temporary (Figure S4).

To better understand the neurochemical changes in the PFOS-exposed brain, we performed an untargeted MWAS on isolated heads of 3-dpf control and 28 μM PFOS-exposed larvae. Several features were significantly up-regulated or down-regulated between the control and exposed groups (Figure S5). Significantly different metabolites from the MWAS were further analyzed for pathway enrichment using MetaboAnalystR.⁷² Several of the significantly enriched pathways, including glutamate metabolism, aspartate and asparagine metabolism, tyrosine metabolism, and phosphoinositide metabolism, are involved in neuronal excitation, catecholamine synthesis, and neurotransmitter release, uptake, and recycling (Figure S5C; Table S4).

We next sought to determine whether the neurochemical imbalances were predictors of abnormal behavioral activity. To first determine whether our exposure paradigm replicated previously reported behavioral hyperactivity, we exposed embryos to either 7 μM , 14 μM , or 28 μM PFOS at 4 hpf, and performed light/dark behavioral assays at 3 dpf, 4 dpf, and 5 dpf (Figure

S6A,B). Consistent with previous locomotor assays at 6 dpf,⁴⁸ PFOS-exposed larvae were significantly more responsive to light changes, designated by greater distance traveled within the well at 3 dpf following 28 μM exposure (Figure S6E–H) and 5 dpf following 7 μM and 14 μM exposure (Figure S6N–R). In addition to distance traveled, behavior videos were analyzed to assess the frequency of center avoidance within the wells of a 24-well plate. Similar to the mammalian open-field test, center avoidance in a well is an indication of zebrafish anxiety-like behavior, whereas willingness to cross the center suggests a reduced anxiety-like behavior.⁸² As such, we examined the time each larva spent along the well's edge (anxiety-like) vs. center (exploratory) throughout each light/dark behavioral assay (Figure 4A,B). PFOS-exposed fish had notable and significantly less time spent in the center in all dosed groups at 3 and 5 dpf (Figure 4C–E). Interestingly, although the 7 μM PFOS group were not significantly more active during the light-on cycle at 5 dpf (Figure S6P), they exhibited center avoidance only during the light-on cycle (Figure S7G,H). Likewise, although 14 μM PFOS-exposed larvae exhibited significant center-avoidance behavior at 3 dpf, they did not have more swim activity at 3 dpf (Figure S6H). Further, the 14 μM PFOS group exhibited center-avoidance behavior in both the light and dark cycles at 5 dpf (Figure S7I,J), although they were significantly more active only when the light was on, and not when the light was off (Figure S6P,Q). This suggests that anxiety-like behaviors are separable from swim hyperactivity and supports the need to more thoroughly understand the independent behavioral changes associated with PFOS exposure. Given that anxiety-, fear-, and aversive-like behaviors are regulated by the medial

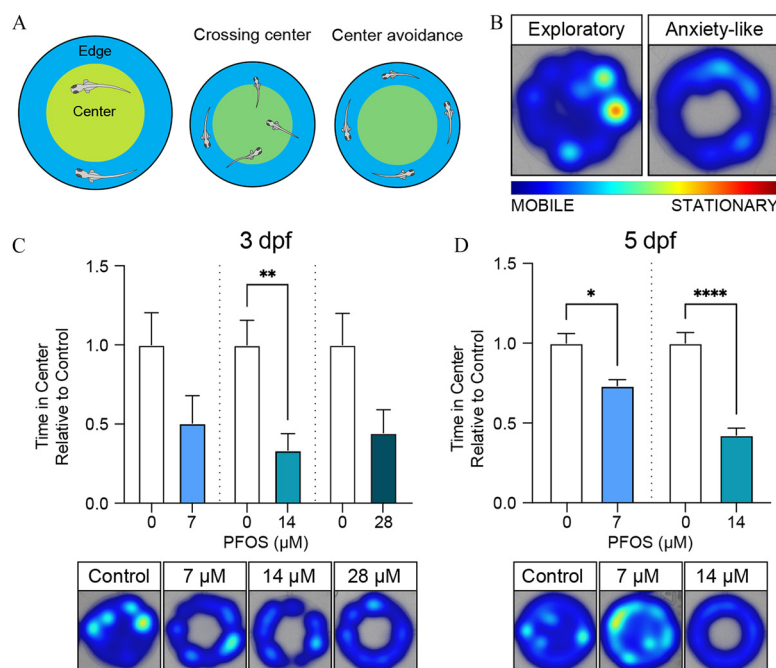


Figure 4. Assessing anxiety-like swim behavior in PFOS-exposed larvae. (A) Larval swim behavior during a 30-min light/dark behavioral assay was used to determine time spent in the well's center (crossing center: less anxious) vs. time spent along the well's edge (center avoidance: more anxious). (B) Heat maps were generated to indicate mobile (blue) vs. stationary (red) swim activity within the well, as well as the zones traversed within the well. (C) Quantification of the time that 3-dpf 7 μM, 14 μM, or 28 μM PFOS-treated larvae spent in the center of the well relative to control-treated larvae. Images are of representative heat maps from each treatment group. (D) Quantification of the time that 5-dpf 7 μM or 14 μM PFOS-treated larvae spent in the center of the well relative to control-treated larvae. Images are of representative heat maps from each treatment group. $n = 76$ –101 fish per group. * $p < 0.05$; ** $p < 0.01$; **** $p < 0.0001$. Error bars represent SEM. See Excel Table S1 for additional statistical details. Note: dpf, days postfertilization; PFOS, perfluorooctane sulfonate; SEM, standard error of the mean.

H in zebrafish,^{83,84} we assessed neuron activity at the H using CaMPARI. Fish exposed to PFOS did not differ in habenular activity at 3 dpf, and only 14 μM PFOS-exposed larvae showed a significant difference in habenular activity at 5 dpf (Figure S8).

Evaluation of Light/Dark Response in Microglia Mutants Exposed to PFOS

Considering the observed shift in microglia state following PFOS exposure, we sought to determine whether PFOS-induced microglial dysfunction during early larval development influenced neuronal excitation and behavior. To do this, we exposed PFOS to zebrafish with a null mutation for *irf8* (*irf8*^{st96/st96}), a gene required for macrophage formation during primitive and transient definitive hematopoiesis.⁶² *Irif8*-mutant larvae lack the earliest embryonic-derived macrophage populations, including microglia.⁶² Control-treated *irf8* mutants had a slight reduction in swim behavior throughout the recording (Figure 5A; gray vs. yellow traces), although were significantly less reactive to the light-to-dark transitions than control-treated wild-type (WT) larvae (Figure 5B; 96.8 ± 8.3 mm moved vs. 71.5 ± 6.8 mm moved). At 5 dpf, both WT and *irf8*-mutant larvae exposed to 8 μM PFOS were significantly more active than control-treated larvae (Figure 5A; Figure S9E–G). However, unlike the control-treated *irf8* mutants, PFOS-exposed mutants did not display a trend toward reduced swim activity during the light/dark behavioral assay (Figure 5A; blue vs. red traces). PFOS-exposed mutants also exhibited the most dramatic behavioral response to the light-to-dark transitions, especially during the second dark cycle (Figure 5B; minute 15). In addition, although WT control larvae and WT PFOS-exposed larvae had a 14.9% and 23.8% reduction in swim activity by the end of the assay (minute 30), respectively, PFOS-exposed *irf8* mutants had a 47.6% reduction in activity (Figure 5B). PFOS-exposed fish also exhibited higher

expression of neuronal-driven CaMPARI in microglia-deficient larvae, but this was not significant between genotypes (Figure 5C).

Microglia Response to Brain Injury following Optogenetic Modulation of Neuronal Activity

Given the bidirectional communication between microglia and neurons and that microglia state can be modulated by neural activity, we asked whether elevated neural activity alone was sufficient to modify microglial responses to injury. To test this hypothesis, 3-dpf larvae were treated with 5 mM PTZ to increase neuronal activity, then they were injured in the right telencephalon, as described above. PTZ-induced neuronal hyperactivity significantly increased the microglia response at 4 hpi, similar to that of PFOS-exposed larvae (Figure S10). We next asked whether inhibiting neuronal activity in PFOS-exposed larvae using optogenetics could normalize the observed hyperresponsive microglial phenotype. Larvae expressing *Tg(elavl3:Gal4;cryaa:RFP;UAS:eNpHR3.0;mpeg1:EGFP)*, which have pan-neuronal expression of halorhodopsin, as well as GFP-labeled macrophages, were exposed to either a control solution or 28 μM PFOS at 4 hpf. After brain injury at 3 dpf, larvae were either left unstimulated or stimulated for 4 h with 570-nm light to silence neuronal activity. Microglia of unstimulated PFOS-exposed larvae were 34.5% more responsive to injury (Figure 6E,F,I). Conversely, neuronal hyperpolarization rescued microglia hyperresponsiveness, resulting in a 6.6% decrease in microglia response in stimulated PFOS-exposed larvae compared with stimulated controls (Figure 6G–I).

Microglia Response to Brain Injury and Neuronal Network Activity following Chronic Exposure to PFOA, a Known Immunotoxic Congener

To further assess whether microglia hyperresponsiveness following PFOS exposure is a result of neuronal hyperactivity, we

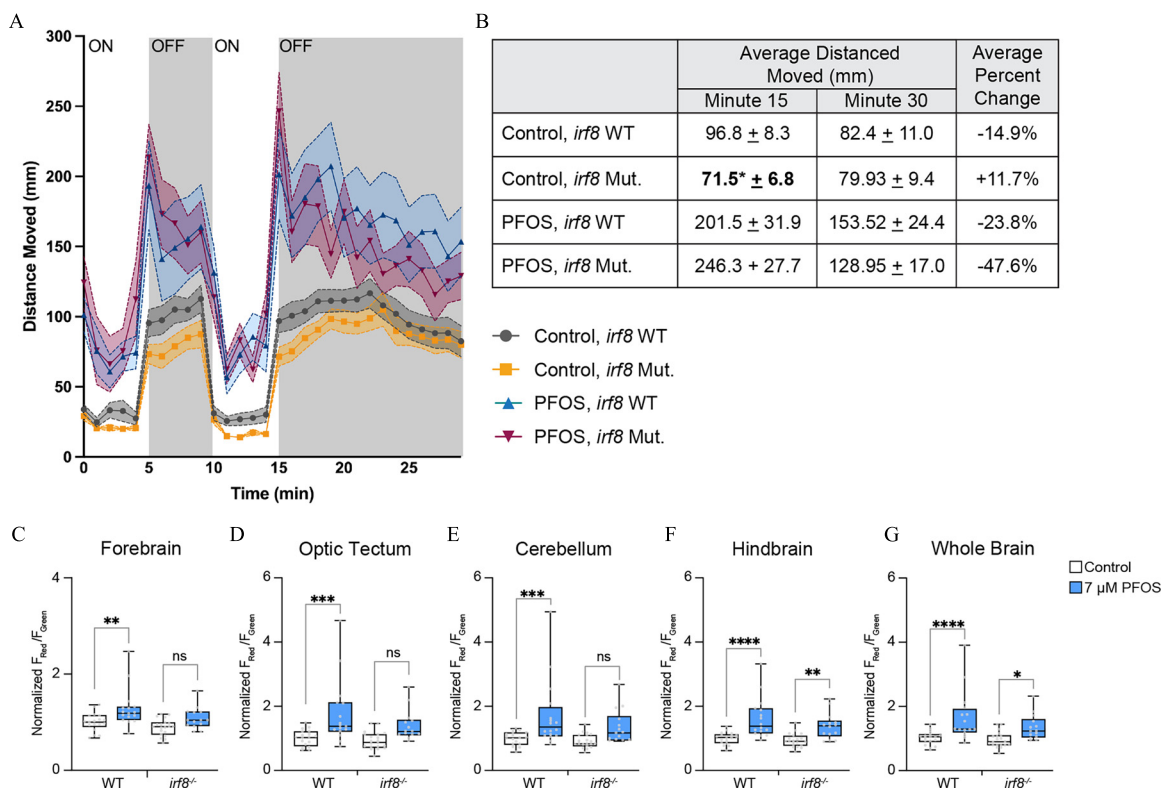


Figure 5. Light/dark behavioral assay and neuronal activity in microglia mutants exposed to PFOS. Wild-type (WT) and microglia-deficient *irf8*^{sr96/sr96} larvae dosed with either control or 7 μ M PFOS were assessed for potential changes in swim behavior and neuronal activity. (A) Light/dark behavioral assay of 5-dpf WT or *irf8*^{-/-} mutant control or PFOS-exposed larvae. (B) Assessment of the average distance moved of 5-dpf larvae at minute 15, which is the start of the second light-off cycle, at minute 30, which is the end of the second light-off cycle, and the percentage change in distance moved from minute 15 to minute 30. (C) Quantification of neuronal CaMPARI activity in the forebrain of 5-dpf control-treated WT, PFOS-treated WT, control-treated mutant, and PFOS-treated mutant larvae. (D) Quantification of neuronal CaMPARI activity in the optic tectum. (E) Quantification of neuronal CaMPARI activity in the cerebellum. (F) Quantification of neuronal CaMPARI activity in the hindbrain. (G) Quantification of neuronal CaMPARI activity in the whole brain. $n = 14$ –22 fish per group for behavior; $n = 13$ –16 fish per group for neuroimaging. ** $p < 0.01$; *** $p < 0.001$; **** $p < 0.0001$. Error bars represent standard deviation. Box plot limits represent 25th to 75th percentile, with the midline representing the median. See Excel Table S1 for additional statistical details. Note: CaMPARI, calcium-modulated photoactivatable ratiometric integrator; Ce, cerebellum; dpf, days postfertilization; FB, forebrain; HB, hindbrain; OT, optic tectum; PFOS, perfluorooctane sulfonate; WB, whole brain.

exposed larval zebrafish to a structurally similar PFAS congener, perfluorooctanoic acid (PFOA). Whereas PFOS has a sulfonic acid head group, PFOA is an 8-carbon PFAS with a carboxylic acid head group. Following the same exposure paradigm used for PFOS exposure (Figure 1A), zebrafish embryos were dosed with either a control solution (0.1% DMSO) or 64 μ M PFOA at 4 hpf. Exposure to 64 μ M PFOA did not result in differing swim behavior during light/dark behavioral assays at 5 dpf (Figure S11A–D). Although PFOA-exposed larvae had shorter body length, there were no observable gross morphological effects on the spine that would affect swimming ability (Figure S12). Using neuronally driven CaMPARI, PFOA exposure did not result in any regional or global differences in neuronal network activity in 5-dpf larvae (Figure 7A–C), unlike the PFOS-exposed groups at this time point (Figure 3). Given that PFOA did not result in neuronal hyperactivity, we asked whether PFOA exposure affected microglial responses to brain injury. Indeed, PFOA exposure did not result in differing microglial responses to brain injury (Figure 7D–F).

Discussion

For more than two decades, researchers have revealed the many biologic, ecologic, and environmental ramifications of PFOS toxicity, as well as the toxicity profiles for a subset of other forever chemical congeners. Here, we used a combination of *in vivo*

imaging of cellular behavior, functional neuroimaging, optogenetic modulation, and behavioral assays to address the impact of PFOS exposure on microglia–neuron interactions and activity in larval zebrafish. Our data demonstrate that developmental PFOS exposure modulated microglia state and induced hyperactivity in response to injury independent of cell death or inflammation. Given that the homeostatic microglia membrane potential is largely maintained by chloride channel currents,⁸⁰ we asked whether activating the optogenetic chloride channel halorhodopsin (eNpHR3.0) could rescue microglia hyperresponsiveness. Indeed, electrical modulation of microglia was sufficient to revert microglia from an amoeboid to a homeostatic morphology and normalize their responses to injury, suggesting electrical dysfunction as a previously underappreciated pathway worth interrogating when studying microglia state and immunotoxicity. PFOS-exposed larvae also exhibited global and regional increases in neuronal activity and anxiety-like behaviors, a previously unidentified neurodevelopmental phenotype of PFOS exposure in zebrafish, with only nominal and temporary impacts on regional brain morphology. We demonstrated that PFOS-induced neuronal hyperactivity was a key mediator of microglia reactivity and that optogenetic silencing of neurons was sufficient to normalize microglia responses to injury. Further, exposure to PFOA did not result in neuronal hyperactivity nor microglia hyperresponsiveness. Together, this study provides, to our knowledge, the first detailed account of the effects of PFOS exposure on the developing

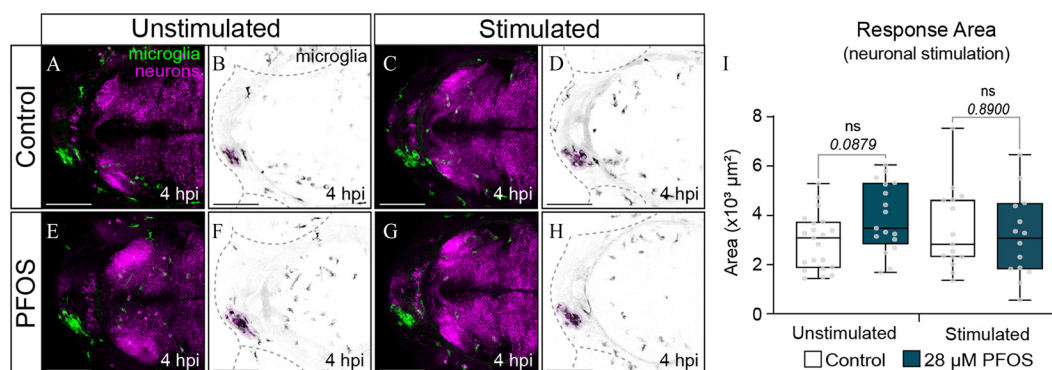


Figure 6. Microglia response to brain injury following optogenetic silencing of neurons in PFOS-exposed larvae. (A) Confocal micrograph of a 3-dpf control-treated larval brain with fluorescently labeled microglia in green and halorhodopsin⁺ neurons in magenta. Image taken 4 hpi without light stimulation. (B) Isolated microglia from (A), pseudocolored in black and white. Area of microglia response 4 hpi shaded with magenta. (C) Confocal micrograph of a 3-dpf control-treated larval brain with fluorescently labeled microglia in green and halorhodopsin⁺ neurons in magenta. Image taken 4 hpi following stimulation with 589-nm light. (D) Isolated microglia from (C), pseudocolored in black and white. (E) Confocal micrograph of a 3-dpf 28 μM PFOS-treated larval brain with fluorescently labeled microglia in green and halorhodopsin⁺ neurons in magenta. Image taken 4 hpi without light stimulation. (F) Isolated microglia from (E), pseudocolored in black and white. (G) Confocal micrograph of a 3-dpf 28 μM-treated larval brain with fluorescently labeled microglia in green and halorhodopsin⁺ neurons in magenta. Image taken 4 hpi following stimulation with 589-nm light. (H) Isolated microglia from (G), pseudocolored in black and white. (I) Quantification of the area of microglia response around the injury site at 4 hpi, as shown by the magenta overlays. $n = 14$ –20 fish per group. Error bars represent standard deviation. Box plot limits represent 25th to 75th percentile, with the midline representing the median. See Excel Table S1 for additional statistical details. Note: dpf, days postfertilization; hpi, hours post-injury; ns, not significant; PFOS, perfluorooctane sulfonate.

brain *in vivo* and adds neuronal hyperactivity as an important end point to assess when studying the impact of toxicant exposures on microglia function.

Zebrafish have long been considered excellent models to study innate immune development and function,^{85,86} including to understand neuro-immune interactions.⁸⁷ Although the immunotoxic impact of PFOS on adaptive immunity has been well documented,⁸⁸ the effects on the innate immune arm are less understood and, at times, contradictory. Studies showing either innate immune activation or suppression following PFOS exposure are likely attributed to varying exposure paradigms, PFOS concentration, animal model, age, or cell line used.^{24,26,28,89,90} The innate immune system is highly sensitive to both endogenous and xenobiotic stimuli and reacts rapidly, creating a signaling cascade that informs all downstream immune functions.⁹¹ Macrophages in particular have the ability to dynamically polarize from a homeostatic state to be pro- or anti-inflammatory depending on the environmental needs. As antigen-presenting cells, macrophages also have the vital role of instructing adaptive immune cells on their responses.⁹¹ The dependency of the adaptive immune system on the innate emphasizes the need to clarify the immunotoxic mechanisms of pollutants, such as PFOS.

This work constitutes the first *in vivo* analysis of microglia, the resident immune population of the CNS, following PFAS exposure. Previous *in vitro* studies using immortalized microglia cell lines suggested PFOS exposure decreased microglial viability, mitochondrial stability, and increased reactive oxygen species (ROS) production *in vitro* in a concentration-dependent manner.^{92,93} We found that PFOS exposure altered the microglia state, demonstrated by their morphological transition from ramified to amoeboid shaped, as well as by the up-regulation of the microglia activation gene *p2ry12*, a purinergic receptor that responds to ATP. It has been previously demonstrated that microglia response to injury is mediated by glutamate-evoked calcium waves and ATP release from the injury site⁷⁸; therefore, ATP released by the injury site and/or through high neuronal activity could be contributing to the microglial hyperresponsiveness in PFOS-exposed larvae. It is still unclear to what extent PFOS is acting directly on the microglia or indirectly through neuronal activation. Microglia activation and injury responses were attenuated by both microglia and neuronal optogenetic silencing,

suggesting that the neuronal environment has a significant influence on the microglia. Of note, although larvae with neuron-driven halorhodopsin had a 34.5% higher microglial response to injury following PFOS exposure, the response was not as significant as it was in other genetic backgrounds ($p = 0.0879$). This is likely due to the fact that optogenetic channels and pumps are highly sensitive, and although we reduced potential exposure to ambient light, leakiness of these opsins may contribute to low-level ion exchange. More work on the baseline permeability of optogenetic channels in a controlled and cell-specific context is needed.

Although, to our knowledge, we are providing the first demonstration of microglial dysfunction in response to toxicant exposure, a shift away from a homeostatic microglia state has been well documented in disease models of various neuropathological states.^{37,38,79,94–97} In addition, pharmacological manipulation of the microglia state or prevention of microglia depletion has been shown to lead to cognitive and functional improvements in some neurological disease models.^{37,38,98} However, it is worth noting that modulation of microglia state is not inherently pathological. For example, microglia depletion following stroke significantly increased infarct size, neuronal cell death, and caused calcium overload.⁹⁹ Microglia depletion during acute seizures also exacerbated excitotoxicity and seizure sensitivity.¹⁰⁰ In addition, the regional specificity of microglia state in a mouse model of chronic stress was considered a protective and/or adaptive response.¹⁰¹ Last, it is important to note that the dosing paradigm used in this study has been shown to impact other organ systems, such as the pancreas.⁶³ Therefore, one cannot dismiss the potential for systemic effects contributing to the neurochemical imbalances or altered microglia state. Although our time-lapse imaging videos, cell death and inflammation data, and microglia quantifications do not suggest macrophages are recruited from the periphery to the brain injury site, more extensive analysis using cell lineage tracing from the periphery would need to be performed to confirm this. However, the potential for the periphery to impact brain health further emphasizes the benefit of understanding systems-level interactions when studying PFAS exposure.

Owing to the developmental and homeostatic roles microglia have in maintaining the excitatory-inhibitory balance,¹⁰² as well as the situation-specific adverse effects that changes in microglia

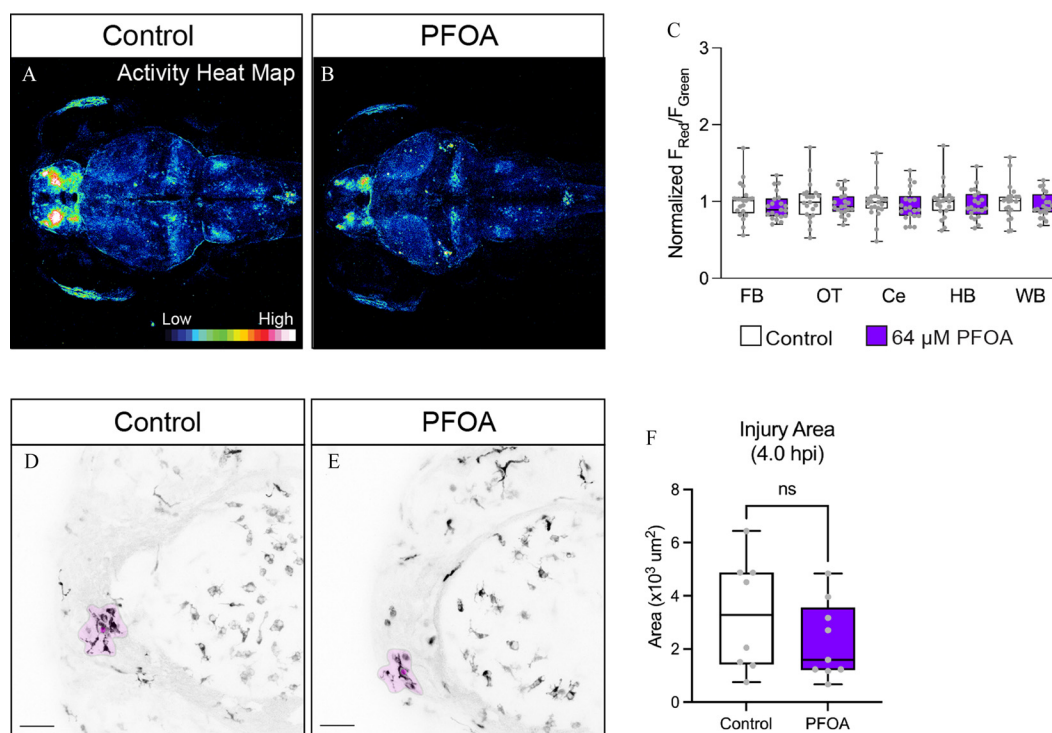


Figure 7. Neuronal activity and microglia response to brain injury following exposure to PFOA, a known immunotoxic congener. PFOA is an 8-carbon PFAS compound with a carboxylate head group. To observe the effects of PFOA on neuronal activity, we again used larvae of the *Tg(elavl3:CaMPARI)* background. (A) Representative heat map of neuronal activity of a 5-dpf control-treated larval brain. (B) Representative heat map of neuronal activity of a 5-dpf 64 μ M PFOA-treated larval brain. (C) Quantification of the regional and global (i.e., WB) neuronal activity as normalized F_{Red}/F_{Green} ratios of 5-dpf control or 64 μ M PFOA-treated larvae. (D) Confocal micrograph of a 3-dpf control-treated larval brain with fluorescently labeled microglia. Image taken 4 hpi, with area of responding microglia shaded in magenta. (E) Confocal micrograph of a 3-dpf 64 μ M PFOA-treated larval brain with fluorescently labeled microglia. Image taken 4 hpi. (F) Quantification of the area of microglia response around the injury site at 4 hpi, as shown by the magenta overlays. $n = 8-9$ fish per group. Error bars represent standard deviation. Box plot limits represent 25th to 75th percentile, with the midline representing the median. See Excel Table S1 for additional statistical details. Note: Ce, cerebellum; dpf, days postfertilization; FB, forebrain; HB, hindbrain; hpi, hours post-injury; ns, not significant; OT, optic tectum; PFAS, per- and polyfluoroalkyl substances; PFOA, perfluorooctanoic acid; WB, whole brain.

state may have on the CNS, we asked whether modulation of microglia state following PFOS exposure was contributing to the behavioral or neuronal hyperactivity. Using microglia-deficient zebrafish with a mutation in the gene *irf8*, we found that control-treated *irf8* mutants had a slight but consistent reduction in swim behavior that was not seen in the PFOS-treated mutants. In addition, PFOS-exposed mutants had the greatest response to the light/dark transition, suggesting that microglia may actually attempt to repress PFOS-induced behavioral hyperactivity. Heightened reactivity may also result in behaviors that impair swim ability, such as seizing or convulsions. Although microglia loss did not affect baseline neuronal calcium signaling, it is worth noting that microglia loss is distinct from microglial dysfunction, and thus it does not rule out the contribution of microglia to neuronal hyperactivity in this context. For example, signals derived from dysfunctional microglia could impact neuronal firing and perhaps swim behavioral responses, which would not be recapitulated in a model of microglial loss. In addition, microglia increasingly accumulate in synaptic regions between 7 and 28 dpf in zebrafish,¹⁰³ suggesting that any significant death-dependent or activity-dependent neuronal pruning may occur developmentally later than the time points investigated in this study. Last, the concentrations of PFOS used in this study might increase neuronal activity too substantially or even irreversibly, such that electrical modulation or loss of microglia is not sufficient to influence the activity in a measurable way.

To our knowledge, this is the first report of *in vivo* neuronal hyperactivity caused by embryonic PFOS exposure. We show that embryonic PFOS exposure resulted in higher intracellular

calcium concentrations across multiple brain regions at various concentrations (7 μ M, 14 μ M, and 28 μ M) and time points (3 dpf and 5 dpf). Both gestational and adult PFOS exposures have been shown to impact calcium-dependent signaling molecules important for memory, including calcium ion/calmodulin-dependent kinase II (CaMKII) and cyclic AMP response element-binding protein (CREB) in rats,¹⁰⁴ suggesting that disrupted calcium signaling is an important mediator of PFOS-induced neurotoxicity. *In vitro* studies also linked PFOS toxicity to disrupted calcium homeostasis.^{51,105} Although the underlying mechanisms remain unknown, possible explanations include increased influx through activation of L-type calcium ion channels¹⁰⁵ and release of intracellular calcium stores through interaction with ryanodine and inositol 1,4,5-trisphosphate receptors.⁵¹ Intracellular calcium excess in neurons promotes excitotoxicity and can cause brain damage leading to various neurological and neurodegenerative disorders,^{106,107} emphasizing the need to further understand the influence of PFAS on neuronal function. PFAS compounds have also been shown to activate peroxisome proliferator-activated receptors (PPARs) *in vitro*, as well as in zebrafish.^{108,109} PPAR γ , in particular, is expressed in neurons, microglia, and astrocytes and mediates inflammatory responses in the CNS.¹¹⁰ Interrogating PPAR activation in the CNS following PFOS exposure could also provide important information about the specific pathways impacted by exposure.

The susceptibility of the developing human brain to PFOS remains a contentious point owing to conflicting data. Although some studies have demonstrated significant correlations between developmental PFOS exposure and ADHD incidence,^{40,41} others

found no such relationship.^{42–45} In the mouse brain, PFOS concentrations have been shown to increase over time and lead to tonic convulsions, despite a lack of morphological phenotypes.¹¹¹ The heightened regional and global network activity demonstrated in this study warrants an assessment of convulsive phenotypes and seizure activity. Although outside the scope of this study, determining the threshold and timescale at which neuronal hyperactivity increases incidence of convulsion would be interesting to pursue.

Similar to previous reports,^{48–50} we observed hyperactive swim behavior in PFOS-exposed larvae during light/dark behavioral assays. However, we are, to our knowledge, the first to report PFOS-induced hyperactivity during the light and dark phases prior to 6 dpf. Hyperactive behavioral changes corresponded well with increased intracellular neuronal calcium concentrations. Of note, increased anxiety-like behaviors were separable from increased swim activity at 3 dpf and 5 dpf and was also specific to light or dark cycles, depending on PFOS concentration. This suggests that there may be further disruptions in neuronal communication beyond just increased calcium concentrations influencing swim activity. In-depth regional brain activity analyses, possibly through the integration of developed analytical pipelines,¹¹² could provide further insight into how PFOS-induced neural activation is linked to behavioral abnormalities in the larval zebrafish.

We identify increased anxiety-like behaviors as a novel phenotype of PFOS neurotoxicity in the larval zebrafish using an adapted open-field test model.^{113–115} Anxiety is an associated symptom of several neurobehavioral disorders linked to PFAS exposures, including autism spectrum disorder and ADHD.^{45,116–118} PFOS-induced center avoidance has been observed in mice exposed during adulthood,¹¹⁹ but developmental anxiety-like behavior has not been previously reported. Of note, previous published research reporting PFOS-induced larval hyperactivity used 96-well plates for higher throughput;^{48,50} however, smaller well sizes may not be conducive to conducting anxiety-like behavioral analyses. We therefore conducted behavioral experiments using 24-well plates, which allowed us to define regions within the well to quantify where fish spent their time swimming. Because dysregulation of habenular activity has been associated with increased anxiety, depression, and fear across species, including the zebrafish,^{83,84,120} we assessed whether neuronal calcium was affected in the H following PFOS exposure. Although only the 14 μ M PFOS group showed neuronal dysregulation at the H, all groups displayed anxiety-like behaviors. This suggests that the H may be but one region dictating anxiety-like responses in larval zebrafish or that temporal differences in habenular activity, not captured using CaMPARI, contribute to anxiety-like responses.

Not only does this study provide the first *in vivo* assessment of neuronal calcium activity following PFOS exposure, but it is also the first, to our knowledge, to evaluate PFOA exposure in this context. The chemical structure of PFOA is similar to PFOS, differing only by the presence of a carboxylic acid head group, rather than sulfonic acid, respectively. PFOA has been shown to cause significant health effects, including immunotoxicity, elevated cholesterol, dysregulated liver metabolism, kidney dysfunction, thyroid disease, among many others.¹²¹ Previous reports using larval zebrafish have found that PFOA concentrations ranging from 4.4 μ M to 80 μ M did not result in a significant difference in 6 dpf swim behavior during the light/dark behavioral assays.⁴⁸ At the concentrations and time points tested here, PFOA exposure did not result in heightened larval swim behavior or neuronal network activity. However, others have reported that 5-dpf larvae exposed to 1 μ M PFOA,¹²² as well as 14 dpf larvae exposed to 2 μ M PFOA,⁵⁰ did result in swim hyperactivity. In addition, although neonatal exposure to PFOA in mice has been shown to result in abnormal

expression of proteins important for brain growth and neuron function,⁴⁶ PFOA exposure of rat primary cortical neurons did not affect spontaneous neuronal activity or burst duration.¹²³ Further analysis is needed to clarify the extent to which PFOA, and other shorter chain length or carboxylic group PFAS, could be neurotoxic or contribute to neural dysregulation. Nevertheless, that PFOA-exposed larvae had normal microglia responses to injury, compared with those exposed to PFOS, further highlights the role of neuronal activity on microglia function.

This study provides the first *in vivo* analysis of how developmental PFOS exposure disrupts larval brain health and function. It also highlights the relevance of understanding pollution-induced effects on innate immune cells, in both a noncanonical developmental and homeostatic context, as well as considering the long-term consequences of potential antigen-presentation dysfunction. In summary, the complexity of neural cell communication, especially during the sensitive period of brain development, emphasizes the importance of studying pollutant exposure in nonisolated systems.

Acknowledgments

We thank W. Talbot for sharing their *irf8^{st96/st96}* mutant line with us. We also thank R. Cyr for excellent care and oversight of our zebrafish facility. Thank you to other members of the Plavicki lab for their discussions in input during various stages of this study. Last, we thank the undergraduate trainees who were involved in the early coordination of this work, namely, R. Dhillon-Richardson and R. Patel.

This work was supported by a National Institutes of Health/National Institute of Environmental Health Science (NIH/NIEHS) Outstanding New Environmental Scientist (ONES) award, as well as cardiopulmonary vascular COBRE Phase II (2PG20GM103652), awarded to J.S.P. In addition, this work was supported by the Ruth L. Kirschstein Predoctoral Individual National Research Service Award (NRSA; F31HL156460) by the NIH/National Heart, Lung, and Blood Institute awarded to S.E.P. S.E.P. and N.R.M. were previously supported by a Brown University Environmental Pathology Training Grant (T32ES007272-26) from NIEHS. The Thermo Liquid Chromatography Orbitrap Mass Spectrometry was partially funded by National Science Foundation Major Research Instrumentation award CBET-1919870 to K.P. (primary investigator) and J.S.P. (co-investigator).

References

- Bullard RD. 1994. Overcoming racism in environmental decisionmaking. *Environment* 36(4):10–44, <https://doi.org/10.1080/00139157.1994.9929997>.
- Muller C, Sampson RJ, Winter AS. 2018. Environmental inequality: the social causes and consequences of lead exposure. *Annu Rev Sociol* 44(1):263–282, <https://doi.org/10.1146/annurev-soc-073117-041222>.
- Liu J, Clark LP, Bechle MJ, Hajat A, Kim SY, Robinson AL, et al. 2021. Disparities in air pollution exposure in the United States by race/ethnicity and income, 1990–2010. *Environ Health Perspect* 129(12):127005, PMID: 34908495, <https://doi.org/10.1289/EHP8584>.
- Kannan K, Corsolini S, Falandysz J, Fillmann G, Kumar KS, Loganathan BG, et al. 2004. Perfluorooctanesulfonate and related fluorochemicals in human blood from several countries. *Environ Sci Technol* 38(17):4489–4495, PMID: 15461154, <https://doi.org/10.1021/es0493446>.
- Paul AG, Jones KC, Sweetman AJ. 2009. A first global production, emission, and environmental inventory for perfluorooctane sulfonate. *Environ Sci Technol* 43(2):386–392, PMID: 19238969, <https://doi.org/10.1021/es802216n>.
- OECD (Organisation for Economic Co-operation and Development). 2020. OECD portal on per and polyfluorinated chemicals. <https://www.oecd.org/chemicalsafety/portal-perfluorinated-chemicals/> [accessed 9 October 2022].
- Buck RC, Franklin J, Berger U, Conder JM, Cousins IT, de Voogt P, et al. 2011. Perfluoroalkyl and polyfluoroalkyl substances in the environment: terminology, classification, and origins. *Integr Environ Assess Manag* 7(4):513–541, PMID: 21793199, <https://doi.org/10.1002/ieam.258>.

8. Gomis MI, Vestergren R, Borg D, Cousins IT. 2018. Comparing the toxic potency in vivo of long-chain perfluoroalkyl acids and fluorinated alternatives. *Environ Int* 113:1–9, PMID: 29421396, <https://doi.org/10.1016/j.envint.2018.01.011>.
9. Chambers WS, Hopkins JG, Richards SM. 2021. A review of per- and polyfluorinated alkyl substance impairment of reproduction. *Front Toxicol* 3:732436, PMID: 35295153, <https://doi.org/10.3389/ftox.2021.732436>.
10. Langenbach B, Wilson M. 2021. Per- and polyfluoroalkyl substances (PFAS): significance and considerations within the regulatory framework of the USA. *Int J Environ Res Public Health* 18(21):11142, PMID: 34769660, <https://doi.org/10.3390/ijerph182111142>.
11. Sunderland EM, Hu XC, Dassuncao C, Tokranov AK, Wagner CC, Allen JG. 2019. A review of the pathways of human exposure to poly- and perfluoroalkyl substances (PFASs) and present understanding of health effects. *J Expo Sci Environ Epidemiol* 29(2):131–147, PMID: 30470793, <https://doi.org/10.1038/s41370-018-0094-1>.
12. Zeng Z, Song B, Xiao R, Zeng G, Gong J, Chen M, et al. 2019. Assessing the human health risks of perfluorooctane sulfonate by in vivo and in vitro studies. *Environ Int* 126:598–610, PMID: 30856447, <https://doi.org/10.1016/j.envint.2019.03.002>.
13. DeWitt JC, Copeland CB, Luebke RW. 2009. Suppression of humoral immunity by perfluorooctanoic acid is independent of elevated serum corticosterone concentration in mice. *Toxicol Sci* 109(1):106–112, PMID: 19240040, <https://doi.org/10.1093/toxsci/kfp040>.
14. DeWitt JC, Peden-Adams MM, Keller JM, Germolec DR. 2012. Immunotoxicity of perfluorinated compounds: recent developments. *Toxicol Pathol* 40(2):300–311, PMID: 22109712, <https://doi.org/10.1177/0192623311428473>.
15. DeWitt JC, Shnyra A, Badr MZ, Loveless SE, Hoban D, Frame SR, et al. 2009. Immunotoxicity of perfluorooctanoic acid and perfluorooctane sulfonate and the role of peroxisome proliferator-activated receptor alpha. *Crit Rev Toxicol* 39(1):76–94, PMID: 18802816, <https://doi.org/10.1080/10408440802209804>.
16. DeWitt JC, Williams WC, Creech NJ, Luebke RW. 2016. Suppression of antigen-specific antibody responses in mice exposed to perfluorooctanoic acid: role of PPAR α and T- and B-cell targeting. *J Immunotoxicol* 13(1):38–45, PMID: 25594567, <https://doi.org/10.3109/1547691X.2014.996682>.
17. Stein CR, McGovern KJ, Pajak AM, Maglione PJ, Wolff MS. 2016. Perfluoroalkyl and polyfluoroalkyl substances and indicators of immune function in children aged 12–19 y: National Health and Nutrition Examination Survey. *Pediatr Res* 79(2):348–357, PMID: 26492286, <https://doi.org/10.1038/pr.2015.213>.
18. Braun JM. 2017. Early-life exposure to EDCs: role in childhood obesity and neurodevelopment. *Nat Rev Endocrinol* 13(3):161–173, PMID: 27857130, <https://doi.org/10.1038/nrendo.2016.186>.
19. Chang ET, Adami HO, Boffetta P, Wedner HJ, Mandel JS. 2016. A critical review of perfluorooctanoate and perfluorooctanesulfonate exposure and immunological health conditions in humans. *Crit Rev Toxicol* 46(4):279–331, PMID: 26761418, <https://doi.org/10.3109/10408444.2015.1122573>.
20. Grandjean P, Andersen EW, Budtz-Jørgensen E, Nielsen F, Mølbaek K, Weihe P, et al. 2012. Serum vaccine antibody concentrations in children exposed to perfluorinated compounds. *JAMA* 307(4):391–397, PMID: 22274686, <https://doi.org/10.1001/jama.2011.2034>.
21. Grandjean P, Heilmann C, Weihe P, Nielsen F, Mogensen UB, Timmermann A, et al. 2017. Estimated exposures to perfluorinated compounds in infancy predict attenuated vaccine antibody concentrations at age 5-years. *J Immunotoxicol* 14(1):188–195, PMID: 28805477, <https://doi.org/10.1080/1547691X.2017.1360968>.
22. Peden-Adams MM, Keller JM, Eudaly JG, Berger J, Gilkeson GS, Keil DE. 2008. Suppression of humoral immunity in mice following exposure to perfluorooctane sulfonate. *Toxicol Sci* 104(1):144–154, PMID: 18359764, <https://doi.org/10.1093/toxsci/kfn059>.
23. NTP (National Toxicology Program). 2016. Immunotoxicity Associated with Exposure to Perfluorooctanoic acid and perfluorooctane sulfonate. https://ntp.niehs.nih.gov/ntp/ohat/pfoa_pfos/pfoa_pfosmonograph_508.pdf [accessed 23 August 2022].
24. Castaño-Ortiz JM, Jaspers VLB, Waugh CA. 2019. PFOS mediates immunomodulation in an avian cell line that can be mitigated via a virus infection. *BMC Vet Res* 15(1):214, PMID: 31238913, <https://doi.org/10.1186/s12917-019-1953-2>.
25. Keil DE, Mehlmann T, Butterworth L, Peden-Adams MM. 2008. Gestational exposure to perfluorooctane sulfonate suppresses immune function in B6C3F1 mice. *Toxicol Sci* 103(1):77–85, PMID: 18252804, <https://doi.org/10.1093/toxsci/kfn015>.
26. Ryu MH, Jha A, Ojo OO, Mahood TH, Basu S, Detillieux KA, et al. 2014. Chronic exposure to perfluorinated compounds: impact on airway hyperresponsiveness and inflammation. *Am J Physiol Lung Cell Mol Physiol* 307(10):L765–L774, PMID: 25217661, <https://doi.org/10.1152/ajplung.00100.2014>.
27. Dong GH, Zhang YH, Zheng L, Liang ZF, Jin YH, He QC. 2012. Subchronic effects of perfluorooctanesulfonate exposure on inflammation in adult male C57BL/6 mice. *Environ Toxicol* 27(5):285–296, PMID: 20737580, <https://doi.org/10.1002/tox.20642>.
28. Qazi MR, Bogdanska J, Butenhoff JL, Nelson BD, DePierre JW, Abedi-Valugerdi M. 2009. High-dose, short-term exposure of mice to perfluorooctanesulfonate (PFOS) or perfluorooctanoate (PFOA) affects the number of circulating neutrophils differently, but enhances the inflammatory responses of macrophages to lipopolysaccharide (LPS) in a similar fashion. *Toxicology* 262(3):207–214, PMID: 19540903, <https://doi.org/10.1016/j.tox.2009.06.010>.
29. Wang LQ, Liu T, Yang S, Sun L, Zhao ZY, Li LY, et al. 2021. Perfluoroalkyl substance pollutants activate the innate immune system through the AIM2 inflammasome. *Nat Commun* 12(1):2915, PMID: 34006824, <https://doi.org/10.1038/s41467-021-23201-0>.
30. Davies LC, Jenkins SJ, Allen JE, Taylor PR. 2013. Tissue-resident macrophages. *Nat Immunol* 14(10):986–995, PMID: 24048120, <https://doi.org/10.1038/ni.2705>.
31. Paolicelli RC, Bolasco G, Pagani F, Maggi L, Scianni M, Panzanelli P, et al. 2011. Synaptic pruning by microglia is necessary for normal brain development. *Science* 333(6048):1456–1458, PMID: 21778362, <https://doi.org/10.1126/science.1202529>.
32. Schafer DP, Lehrman EK, Kautzman AG, Koyama R, Mardinly AR, Yamasaki R, et al. 2012. Microglia sculpt postnatal neural circuits in an activity and complement-dependent manner. *Neuron* 74(4):691–705, PMID: 22632727, <https://doi.org/10.1016/j.neuron.2012.03.026>.
33. Hoshiko M, Arnoux I, Avignone E, Yamamoto N, Audinat E. 2012. Deficiency of the microglial receptor CX3CR1 impairs postnatal functional development of thalamocortical synapses in the barrel cortex. *J Neurosci* 32(43):15106–15111, PMID: 23100431, <https://doi.org/10.1523/JNEUROSCI.1167-12.2012>.
34. Parkhurst CN, Yang G, Nanan I, Savas JN, Yates JR III, Lafaille JJ, et al. 2013. Microglia promote learning-dependent synapse formation through brain-derived neurotrophic factor. *Cell* 155(7):1596–1609, PMID: 24360280, <https://doi.org/10.1016/j.cell.2013.11.030>.
35. Szepesi Z, Manouchehrian O, Bachiller S, Deierborg T. 2018. Bidirectional microglia–neuron communication in health and disease. *Front Cell Neurosci* 12:323, PMID: 30319362, <https://doi.org/10.3389/fncel.2018.00323>.
36. Wake H, Moorhouse AJ, Jinno S, Kohsaka S, Nabekura J. 2009. Resting microglia directly monitor the functional state of synapses *in vivo* and determine the fate of ischemic terminals. *J Neurosci* 29(13):3974–3980, PMID: 19339593, <https://doi.org/10.1523/JNEUROSCI.4363-08.2009>.
37. Pinto B, Morelli G, Rastogi M, Savardi A, Fumagalli A, Petretto A, et al. 2020. Rescuing over-activated microglia restores cognitive performance in juvenile animals of the Dp(16) mouse model of Down syndrome. *Neuron* 108(5):887–904.e12, PMID: 33027640, <https://doi.org/10.1016/j.neuron.2020.09.010>.
38. Mancuso R, Fryatt G, Cleal M, Obst J, Pipi E, Monzón-Sandoval J, et al. 2019. CSF1R inhibitor JNJ-40346527 attenuates microglial proliferation and neurodegeneration in P301S mice. *Brain* 142(10):3243–3264, PMID: 31504240, <https://doi.org/10.1093/brain/awz241>.
39. Hiragi T, Ikegaya Y, Koyama R. 2018. Microglia after seizures and in epilepsy. *Cells* 7(4):26, PMID: 29597334, <https://doi.org/10.3390/cells7040026>.
40. Hoffman K, Webster TF, Weisskopf MG, Weinberg J, Vieira VM. 2010. Exposure to polyfluoroalkyl chemicals and attention deficit/hyperactivity disorder in U.S. children 12–15 years of age. *Environ Health Perspect* 118(12):1762–1767, PMID: 20551004, <https://doi.org/10.1289/ehp.1001898>.
41. Lenters V, Iszatt N, Forns J, Čechová E, Kočan A, Legler J, et al. 2019. Early-life exposure to persistent organic pollutants (OCs, PBDEs, PCBs, PFASs) and attention-deficit/hyperactivity disorder: a multi-pollutant analysis of a Norwegian birth cohort. *Environ Int* 125:33–42, PMID: 30703609, <https://doi.org/10.1016/j.envint.2019.01.020>.
42. Fei C, McLaughlin JK, Lipworth L, Olsen J. 2008. Prenatal exposure to perfluorooctanoate (PFOA) and perfluorooctanesulfonate (PFOS) and maternally reported developmental milestones in infancy. *Environ Health Perspect* 116(10):1391–1395, PMID: 18941583, <https://doi.org/10.1289/ehp.11277>.
43. Lien GW, Huang CC, Shiu JS, Chen MH, Hsieh WS, Guo YL, et al. 2016. Perfluoroalkyl substances in cord blood and attention deficit/hyperactivity disorder symptoms in seven-year-old children. *Chemosphere* 156:118–127, PMID: 27174824, <https://doi.org/10.1016/j.chemosphere.2016.04.102>.
44. Liew Z, Ritz B, von Ehrenstein OS, Bech BH, Nohr EA, Fei C, et al. 2015. Attention deficit/hyperactivity disorder and childhood autism in association with prenatal exposure to perfluoroalkyl substances: a nested case–control study in the Danish National Birth Cohort. *Environ Health Perspect* 123(4):367–373, PMID: 25616253, <https://doi.org/10.1289/ehp.1408412>.
45. Ode A, Källén K, Gustafsson P, Rylander L, Jönsson BAG, Olofsson P, et al. 2014. Fetal exposure to perfluorinated compounds and attention deficit hyperactivity disorder in childhood. *PLoS One* 9(4):e95891, PMID: 24760015, <https://doi.org/10.1371/journal.pone.0095891>.
46. Johansson N, Eriksson P, Viberg H. 2009. Neonatal exposure to PFOS and PFOA in mice results in changes in proteins which are important for neuronal growth and synaptogenesis in the developing brain. *Toxicol Sci* 108(2):412–418, PMID: 19211617, <https://doi.org/10.1093/toxsci/kfp029>.
47. Johansson N, Fredriksson A, Eriksson P. 2008. Neonatal exposure to perfluorooctane sulfonate (PFOS) and perfluorooctanoic acid (PFOA) causes

- neurobehavioural defects in adult mice. *Neurotoxicology* 29(1):160–169, PMID: [18063051](#), <https://doi.org/10.1016/j.neuro.2007.10.008>.
48. Gaballah S, Swank A, Sobus JR, Howey XM, Schmid J, Catron T, et al. 2020. Evaluation of developmental toxicity, developmental neurotoxicity, and tissue dose in zebrafish exposed to GenX and other PFAS. *Environ Health Perspect* 128(4):047005, PMID: [32271623](#), <https://doi.org/10.1289/EHP5843>.
 49. Huang H, Huang C, Wang L, Ye X, Bai C, Simonich MT, et al. 2010. Toxicity, uptake kinetics and behavior assessment in zebrafish embryos following exposure to perfluorooctanesulphonic acid (PFOS). *Aquat Toxicol* 98(2):139–147, PMID: [20171748](#), <https://doi.org/10.1016/j.aquatox.2010.02.003>.
 50. Jantzen CE, Annunziato KM, Cooper KR. 2016. Behavioral, morphometric, and gene expression effects in adult zebrafish (*Danio rerio*) embryonically exposed to PFQA, PFOS, and PFNA. *Aquat Toxicol* 180:123–130, PMID: [27710860](#), <https://doi.org/10.1016/j.aquatox.2016.09.011>.
 51. Liu X, Jin Y, Liu W, Wang F, Hao S. 2011. Possible mechanism of perfluorooctane sulfonate and perfluorooctanoate on the release of calcium ion from calcium stores in primary cultures of rat hippocampal neurons. *Toxicol In Vitro* 25(7):1294–1301, PMID: [21575708](#), <https://doi.org/10.1016/j.tiv.2011.04.016>.
 52. Christou M, Fraser TWK, Berg V, Ropstad E, Kamstra JH. 2020. Calcium signaling as a possible mechanism behind increased locomotor response in zebrafish larvae exposed to a human relevant persistent organic pollutant mixture or PFOS. *Environ Res* 188:109702, PMID: [32474314](#), <https://doi.org/10.1016/j.envres.2020.109702>.
 53. Institute of Laboratory Animal Resources (U.S.), National Research Council (Canada). 2011. *Guide for the Care and Use of Laboratory Animals*. 8th ed. Washington, DC: National Academies Press.
 54. Westerfield M. 2000. *The Zebrafish Book: A Guide for the Laboratory Use of Zebrafish (Brachydanio rerio)*. Eugene, OR: University of Oregon.
 55. Ellett F, Pase L, Hayman JW, Andrianopoulos A, Lieschke GJ. 2011. *mpeg1* promoter transgenes direct macrophage-lineage expression in zebrafish. *Blood* 117(4):e49–e56, PMID: [21084707](#), <https://doi.org/10.1182/blood-2010-10-314120>.
 56. Arrenberg AB, Del Bene F, Baier H. 2009. Optical control of zebrafish behavior with halorhodopsin. *Proc Natl Acad Sci U S A* 106(42):17968–17973, PMID: [19805086](#), <https://doi.org/10.1073/pnas.0906252106>.
 57. Gradinaru V, Zhang F, Ramakrishnan C, Mattis J, Prakash R, Diester I, et al. 2010. Molecular and cellular approaches for diversifying and extending optogenetics. *Cell* 141(1):154–165, PMID: [20303157](#), <https://doi.org/10.1016/j.cell.2010.02.037>.
 58. Fosque BF, Sun Y, Dana H, Yang CT, Ohya T, Tadross MR, et al. 2015. Neural circuits. Labeling of active neural circuits in vivo with designed calcium integrators. *Science* 347(6223):755–760, PMID: [25678659](#), <https://doi.org/10.1126/science.1260922>.
 59. Kimura Y, Satou C, Higashijima S. 2008. V2a and V2b neurons are generated by the final divisions of pair-producing progenitors in the zebrafish spinal cord. *Development* 135(18):3001–3005, PMID: [18684740](#), <https://doi.org/10.1242/dev.024802>.
 60. Sato T, Takahoko M, Okamoto H. 2006. HuC:Kaede, a useful tool to label neural morphologies in networks in vivo. *Genesis* 44(3):136–142, PMID: [16496337](#), <https://doi.org/10.1002/gene.20196>.
 61. Davison JM, Akitake CM, Goll MG, Rhee JM, Gosse N, Baier H, et al. 2007. Transactivation from Gal4-VP16 transgenic insertions for tissue-specific cell labeling and ablation in zebrafish. *Dev Biol* 304(2):811–824, PMID: [17335798](#), <https://doi.org/10.1016/j.ydbio.2007.01.033>.
 62. Shiao CE, Kaufman Z, Meireles AM, Talbot WS. 2015. Differential requirement for *irf8* in formation of embryonic and adult macrophages in zebrafish. *PLoS One* 10(1):e0117513, PMID: [25615614](#), <https://doi.org/10.1371/journal.pone.0117513>.
 63. Sant KE, Jacobs HM, Borofski KA, Moss JB, Timme-Laragy AR. 2017. Embryonic exposures to perfluorooctanesulfonic acid (PFOS) disrupt pancreatic organogenesis in the zebrafish, *Danio rerio*. *Environ Pollut* 220(pt B):807–817, PMID: [27810111](#), <https://doi.org/10.1016/j.envpol.2016.10.057>.
 64. Chen J, Tanguay RL, Tal TL, Gai Z, Ma X, Bai C, et al. 2014. Early life perfluorooctanesulphonic acid (PFOS) exposure impairs zebrafish organogenesis. *Aquat Toxicol* 150:124–132, PMID: [24667235](#), <https://doi.org/10.1016/j.aquatox.2014.03.005>.
 65. Kishimoto N, Shimizu K, Sawamoto K. 2012. Neuronal regeneration in a zebrafish model of adult brain injury. *Dis Model Mech* 5(2):200–209, PMID: [22028327](#), <https://doi.org/10.1242/dmm.007336>.
 66. Schindelin J, Arganda-Carreras I, Frise E, Kaynig V, Longair M, Pietzsch T, et al. 2012. Fiji: an open-source platform for biological-image analysis. *Nat Methods* 9(7):676–682, PMID: [22743772](#), <https://doi.org/10.1038/nmeth.2019>.
 67. Wallace CK, Bright LA, Marx JO, Andersen RP, Mullins MC, Carty AJ. 2018. Effectiveness of rapid cooling as a method of euthanasia for young zebrafish (*Danio rerio*). *J Am Assoc Lab Anim Sci* 57(1):58–63, PMID: [29402353](#).
 68. Delic J, Coppey J, Magdelenat H, Coppey-Moisson M. 1991. Impossibility of acridine orange intercalation in nuclear DNA of the living cell. *Exp Cell Res* 194(1):147–153, PMID: [2015848](#), [https://doi.org/10.1016/0014-4827\(91\)90144-j](https://doi.org/10.1016/0014-4827(91)90144-j).
 69. Yu T, Park Y, Johnson JM, Jones DP. 2009. apLCMS—adaptive processing of high-resolution LC/MS data. *Bioinformatics* 25(15):1930–1936, PMID: [19414529](#), <https://doi.org/10.1093/bioinformatics/btp291>.
 70. Uppal K, Soltow QA, Strobel FH, Pittard WS, Gernert KM, Yu T, et al. 2013. xMSAnalyzer: automated pipeline for improved feature detection and downstream analysis of large-scale, non-targeted metabolomics data. *BMC Bioinformatics* 14:15, PMID: [23323971](#), <https://doi.org/10.1186/1471-2105-14-15>.
 71. Benjamini Y, Hochberg Y. 1995. Controlling the false discovery rate: a practical and powerful approach to multiple testing. *J R Stat Soc Series B Stat Methodol* 57(1):289–300, <https://doi.org/10.1111/j.2517-6161.1995.tb02031.x>.
 72. Chong J, Xia J. 2018. MetaboAnalystR: an R package for flexible and reproducible analysis of metabolomics data. *Bioinformatics* 34(24):4313–4314, PMID: [29955821](#), <https://doi.org/10.1093/bioinformatics/bty528>.
 73. Sud M, Fahy E, Cotter D, Azam K, Vadivelu I, Burant C, et al. 2016. Metabolomics Workbench: an international repository for metabolomics data and metadata, metabolite standards, protocols, tutorials and training, and analysis tools. *Nucleic Acids Res* 44(D1):D463–D470, PMID: [26467476](#), <https://doi.org/10.1093/nar/gkv1042>.
 74. Badimon A, Strasburger HJ, Ayata P, Chen X, Nair A, Ikegami A, et al. 2020. Negative feedback control of neuronal activity by microglia. *Nature* 586(7829):417–423, PMID: [32999463](#), <https://doi.org/10.1038/s41586-020-2777-8>.
 75. Davalos D, Grutzendler J, Yang G, Kim JV, Zuo Y, Jung S, et al. 2005. ATP mediates rapid microglial response to local brain injury in vivo. *Nat Neurosci* 8(6):752–758, PMID: [15895084](#), <https://doi.org/10.1038/nn1472>.
 76. Yu T, Zhang X, Shi H, Tian J, Sun L, Hu X, et al. 2019. P2Y12 regulates microglia activation and excitatory synaptic transmission in spinal lamina II neurons during neuropathic pain in rodents. *Cell Death Dis* 10(3):165, PMID: [30778044](#), <https://doi.org/10.1038/s41419-019-1425-4>.
 77. Schmidt R, Beil T, Strähle U, Rastegar S. 2014. Stab wound injury of the zebrafish adult telencephalon: a method to investigate vertebrate brain neurogenesis and regeneration. *J Vis Exp* (90):e51753, PMID: [25146302](#), <https://doi.org/10.3791/51753>.
 78. Sieger D, Moritz C, Ziegenhals T, Prykhodzij S, Peri F. 2012. Long-range Ca²⁺ waves transmit brain-damage signals to microglia. *Dev Cell* 22(6):1138–1148, PMID: [22632801](#), <https://doi.org/10.1016/j.devcel.2012.04.012>.
 79. Donat CK, Scott G, Gentleman SM, Sastre M. 2017. Microglial activation in traumatic brain injury. *Front Aging Neurosci* 9:208, PMID: [28701948](#), <https://doi.org/10.3389/fnagi.2017.00208>.
 80. Newell EW, Schlichter LC. 2005. Integration of K⁺ and Cl[−] currents regulate steady-state and dynamic membrane potentials in cultured rat microglia. *J Physiol* 567(pt 3):869–890, PMID: [16020460](#), <https://doi.org/10.1113/jphysiol.2005.092056>.
 81. Baraban SC, Taylor MR, Castro PA, Baier H. 2005. Pentylentetrazole induced changes in zebrafish behavior, neural activity and c-fos expression. *Neuroscience* 131(3):759–768, PMID: [15730879](#), <https://doi.org/10.1016/j.neuroscience.2004.11.031>.
 82. Colwill RM, Creton R. 2011. Imaging escape and avoidance behavior in zebrafish larvae. *Rev Neurosci* 22(1):63–73, PMID: [21572576](#), <https://doi.org/10.1515/RNS.2011.008>.
 83. Mathuru AS, Jesuthasan S. 2013. The medial habenula as a regulator of anxiety in adult zebrafish. *Front Neural Circuits* 7:99, PMID: [23750127](#), <https://doi.org/10.3389/fnirc.2013.00099>.
 84. Okamoto H, Agetsuma M, Aizawa H. 2012. Genetic dissection of the zebrafish habenula, a possible switching board for selection of behavioral strategy to cope with fear and anxiety. *Dev Neurobiol* 72(3):386–394, PMID: [21567982](#), <https://doi.org/10.1002/dneu.20913>.
 85. Trede NS, Langenau DM, Traver D, Look AT, Zon LI. 2004. The use of zebrafish to understand immunity. *Immunity* 20(4):367–379, PMID: [15084267](#), [https://doi.org/10.1016/S1074-7613\(04\)00084-6](https://doi.org/10.1016/S1074-7613(04)00084-6).
 86. Galindo-Villegas J. 2016. Recent findings on vertebrate developmental immunity using the zebrafish model. *Mol Immunol* 69:106–112, PMID: [26589453](#), <https://doi.org/10.1016/j.molimm.2015.10.011>.
 87. Levraud JP, Rawls JF, Clatworthy AE. 2022. Using zebrafish to understand reciprocal interactions between the nervous and immune systems and the microbial world. *J Neuroinflammation* 19(1):170, PMID: [35765004](#), <https://doi.org/10.1186/s12974-022-02506-x>.
 88. DeWitt JC, Blossom SJ, Schaidler LA. 2019. Exposure to per-fluoroalkyl and polyfluoroalkyl substances leads to immunotoxicity: epidemiological and toxicological evidence. *J Expo Sci Environ Epidemiol* 29(2):148–156, PMID: [30482935](#), <https://doi.org/10.1038/s41370-018-0097-y>.
 89. Mollenhauer MAM, Bradshaw SG, Fair PA, McGuinn WD, Peden-Adams MM. 2011. Effects of perfluorooctane sulfonate (PFOS) exposure on markers of inflammation in female B6C3F1 mice. *J Environ Sci Health A Tox Hazard Subst Environ Eng* 46(2):97–108, PMID: [21170772](#), <https://doi.org/10.1080/10934529.2011.532418>.

90. Hou YF, Shan C, Zhuang SY, Zhuang QQ, Ghosh A, Zhu KC, et al. 2021. Gut microbiota-derived propionate mediates the neuroprotective effect of osteocalcin in a mouse model of Parkinson's disease. *Microbiome* 9(1):34, PMID: [33517890](https://doi.org/10.1186/s40168-020-00988-6), <https://doi.org/10.1186/s40168-020-00988-6>.
91. Clark R, Kupper T. 2005. Old meets new: the interaction between innate and adaptive immunity. *J Invest Dermatol* 125(4):629–637, PMID: [16185260](https://doi.org/10.1111/j.0022-202X.2005.23856.x), <https://doi.org/10.1111/j.0022-202X.2005.23856.x>.
92. Ge J, Wang C, Nie X, Yang J, Lu H, Song X, et al. 2016. ROS-mediated apoptosis of HAPI microglia through p53 signaling following PFOS exposure. *Environ Toxicol Pharmacol* 46:9–16, PMID: [27414741](https://doi.org/10.1016/j.etap.2016.06.025), <https://doi.org/10.1016/j.etap.2016.06.025>.
93. Zhang L, Li YY, Zeng HC, Li M, Wan YJ, Schluesener HJ, et al. 2011. Perfluorooctane sulfonate induces apoptosis in N9 microglial cell line. *Int J Toxicol* 30(2):207–215, PMID: [21115943](https://doi.org/10.1177/1091581810387832), <https://doi.org/10.1177/1091581810387832>.
94. Chen Z, Jalabi W, Shpargel KB, Farabaugh KT, Dutta R, Yin X, et al. 2012. Lipopolysaccharide-induced microglial activation and neuroprotection against experimental brain injury is independent of hematogenous TLR4. *J Neurosci* 32(34):11706–11715, PMID: [22915113](https://doi.org/10.1523/JNEUROSCI.0730-12.2012), <https://doi.org/10.1523/JNEUROSCI.0730-12.2012>.
95. Dissing-Olesen L, LeDue JM, Rungta RL, Hefendehl JK, Choi HB, MacVicar BA. 2014. Activation of neuronal NMDA receptors triggers transient ATP-mediated microglial process outgrowth. *J Neurosci* 34(32):10511–10527, PMID: [25100586](https://doi.org/10.1523/JNEUROSCI.0405-14.2014), <https://doi.org/10.1523/JNEUROSCI.0405-14.2014>.
96. Echeverry S, Rodriguez MJ, Torres YP. 2016. Transient receptor potential channels in microglia: roles in physiology and disease. *Neurotox Res* 30(3):467–478, PMID: [27260222](https://doi.org/10.1007/s12640-016-9632-6), <https://doi.org/10.1007/s12640-016-9632-6>.
97. Eyo UB, Peng J, Swiatkowski P, Mukherjee A, Bispo A, Wu LJ. 2014. Neuronal hyperactivity recruits microglial processes via neuronal NMDA receptors and microglial P2Y12 receptors after status epilepticus. *J Neurosci* 34(32):10528–10540, PMID: [25100587](https://doi.org/10.1523/JNEUROSCI.0416-14.2014), <https://doi.org/10.1523/JNEUROSCI.0416-14.2014>.
98. Goldfarb S, Feinstein N, Ganz T, Vershkov D, Lachish M, Ben-Hur T. 2021. Electric neurostimulation regulates microglial activation via retinoic acid receptor α signaling. *Brain Behav Immun* 96:40–53, PMID: [33989746](https://doi.org/10.1016/j.bbi.2021.05.007), <https://doi.org/10.1016/j.bbi.2021.05.007>.
99. Szalay G, Martinecz B, Lénárt N, Környei Z, Orsolits B, Judák L, et al. 2016. Microglia protect against brain injury and their selective elimination dysregulates neuronal network activity after stroke. *Nat Commun* 7:11499, PMID: [27139776](https://doi.org/10.1038/ncomms11499), <https://doi.org/10.1038/ncomms11499>.
100. Liu M, Jiang L, Wen M, Ke Y, Tong X, Huang W, et al. 2020. Microglia depletion exacerbates acute seizures and hippocampal neuronal degeneration in mouse models of epilepsy. *Am J Physiol Cell Physiol* 319(3):C605–C610, PMID: [32783655](https://doi.org/10.1152/ajpcell.00205.2020), <https://doi.org/10.1152/ajpcell.00205.2020>.
101. Tynan RJ, Naicker S, Hinwood M, Nalivaiko E, Buller KM, Pow DV, et al. 2010. Chronic stress alters the density and morphology of microglia in a subset of stress-responsive brain regions. *Brain Behav Immun* 24(7):1058–1068, PMID: [20153418](https://doi.org/10.1016/j.bbi.2010.02.001), <https://doi.org/10.1016/j.bbi.2010.02.001>.
102. Henstridge CM, Tzioras M, Paolicelli RC. 2019. Glial contribution to excitatory and inhibitory synapse loss in neurodegeneration. *Front Cell Neurosci* 13:63, PMID: [30863284](https://doi.org/10.3389/fncel.2019.00063), <https://doi.org/10.3389/fncel.2019.00063>.
103. Silva NJ, Dorman LC, Vainchtein ID, Horneck NC, Molofsky AV. 2021. In situ and transcriptomic identification of microglia in synapse-rich regions of the developing zebrafish brain. *Nat Commun* 12(1):5916, PMID: [34625548](https://doi.org/10.1038/s41467-021-26206-x), <https://doi.org/10.1038/s41467-021-26206-x>.
104. Liu X, Liu W, Jin Y, Yu W, Wang F, Liu L. 2010. Effect of gestational and lactational exposure to perfluorooctanesulfonate on calcium-dependent signaling molecules gene expression in rats' hippocampus. *Arch Toxicol* 84(1):71–79, PMID: [19756518](https://doi.org/10.1007/s00204-009-0467-2), <https://doi.org/10.1007/s00204-009-0467-2>.
105. Liao CY, Li XY, Wu B, Duan S, Jiang GB. 2008. Acute enhancement of synaptic transmission and chronic inhibition of synaptogenesis induced by perfluorooctane sulfonate through mediation of voltage-dependent calcium channel. *Environ Sci Technol* 42(14):5335–5341, PMID: [18754390](https://doi.org/10.1021/es800018k), <https://doi.org/10.1021/es800018k>.
106. Armada-Moreira A, Gomes JI, Pina CC, Savchak OK, Gonçalves-Ribeiro J, Rei N, et al. 2020. Going the extra (synaptic) mile: excitotoxicity as the road toward neurodegenerative diseases. *Front Cell Neurosci* 14:90, PMID: [32390802](https://doi.org/10.3389/fncel.2020.00090), <https://doi.org/10.3389/fncel.2020.00090>.
107. Olloquequi J, Cornejo-Córdova E, Verdaguier E, Soriano FX, Binvignat O, Auladell C, et al. 2018. Excitotoxicity in the pathogenesis of neurological and psychiatric disorders: therapeutic implications. *J Psychopharmacol* 32(3):265–275, PMID: [29444621](https://doi.org/10.1177/0269881118754680), <https://doi.org/10.1177/0269881118754680>.
108. Rosen MB, Das KP, Rooney J, Abbott B, Lau C, Corton JC. 2017. PPAR α -independent transcriptional targets of perfluoroalkyl acids revealed by transcript profiling. *Toxicology* 387:95–107, PMID: [28558994](https://doi.org/10.1016/j.tox.2017.05.013), <https://doi.org/10.1016/j.tox.2017.05.013>.
109. Takacs ML, Abbott BD. 2007. Activation of mouse and human peroxisome proliferator-activated receptors (α , β/δ , γ) by perfluorooctanoic acid and perfluorooctane sulfonate. *Toxicol Sci* 95(1):108–117, PMID: [17047030](https://doi.org/10.1093/toxsci/kfl135), <https://doi.org/10.1093/toxsci/kfl135>.
110. Villapol S. 2018. Roles of peroxisome proliferator-activated receptor gamma on brain and peripheral inflammation. *Cell Mol Neurobiol* 38(1):121–132, PMID: [28975471](https://doi.org/10.1007/s10571-017-0554-5), <https://doi.org/10.1007/s10571-017-0554-5>.
111. Sato I, Kawamoto K, Nishikawa Y, Tsuda S, Yoshida M, Yaegashi K, et al. 2009. Neurotoxicity of perfluorooctane sulfonate (PFOS) in rats and mice after single oral exposure. *J Toxicol Sci* 34(5):569–574, PMID: [19797866](https://doi.org/10.2131/jts.34.569), <https://doi.org/10.2131/jts.34.569>.
112. Randlett O, Wee CL, Naumann EA, Nnaemeka O, Schoppik D, Fitzgerald JE, et al. 2015. Whole-brain activity mapping onto a zebrafish brain atlas. *Nat Methods* 12(11):1039–1046, PMID: [26778924](https://doi.org/10.1038/nmeth.3581), <https://doi.org/10.1038/nmeth.3581>.
113. Kaluff AV, Stewart AM. 2012. *Zebrafish Protocols for Neurobehavioral Research*. New York, NY: Humana Press.
114. Ahmad F, Richardson MK. 2013. Exploratory behaviour in the open field test adapted for larval zebrafish: impact of environmental complexity. *Behav Processes* 92:88–98, PMID: [23123970](https://doi.org/10.1016/j.beproc.2012.10.014), <https://doi.org/10.1016/j.beproc.2012.10.014>.
115. Richendrer H, Pelkowski SD, Colwill RM, Cretton R. 2012. On the edge: pharmacological evidence for anxiety-related behavior in zebrafish larvae. *Behav Brain Res* 228(1):99–106, PMID: [22155488](https://doi.org/10.1016/j.bbr.2011.11.041), <https://doi.org/10.1016/j.bbr.2011.11.041>.
116. Skogheim TS, Weyde KVF, Aase H, Engel SM, Surén P, Øie MG, et al. 2021. Prenatal exposure to per- and polyfluoroalkyl substances (PFAS) and associations with attention-deficit/hyperactivity disorder and autism spectrum disorder in children. *Environ Res* 202:111692, PMID: [34293314](https://doi.org/10.1016/j.envres.2021.111692), <https://doi.org/10.1016/j.envres.2021.111692>.
117. Oh J, Bennett DH, Calafat AM, Tancredi D, Roa DL, Schmidt RJ, et al. 2021. Prenatal exposure to per- and polyfluoroalkyl substances in association with autism spectrum disorder in the MARBLES study. *Environ Int* 147:106328, PMID: [33387879](https://doi.org/10.1016/j.envint.2020.106328), <https://doi.org/10.1016/j.envint.2020.106328>.
118. Shin HM, Bennett DH, Calafat AM, Tancredi D, Hertz-Picciotto I. 2020. Modeled prenatal exposure to per- and polyfluoroalkyl substances in association with child autism spectrum disorder: a case-control study. *Environ Res* 186:109514, PMID: [32353786](https://doi.org/10.1016/j.envres.2020.109514), <https://doi.org/10.1016/j.envres.2020.109514>.
119. Fuentes S, Vicens P, Colomina MT, Domingo JL. 2007. Behavioral effects in adult mice exposed to perfluorooctane sulfonate (PFOS). *Toxicology* 242(1–3):123–129, PMID: [17950980](https://doi.org/10.1016/j.tox.2007.09.012), <https://doi.org/10.1016/j.tox.2007.09.012>.
120. Browne CA, Hammack R, Lucki I. 2018. Dysregulation of the lateral habenula in major depressive disorder. *Front Synaptic Neurosci* 10:46, PMID: [30581384](https://doi.org/10.3389/fnsyn.2018.00046), <https://doi.org/10.3389/fnsyn.2018.00046>.
121. Post GB, Cohn PD, Cooper KR. 2012. Perfluorooctanoic acid (PFOA), an emerging drinking water contaminant: a critical review of recent literature. *Environ Res* 116:93–117, PMID: [22560884](https://doi.org/10.1016/j.envres.2012.03.007), <https://doi.org/10.1016/j.envres.2012.03.007>.
122. Rericha Y, Cao D, Truong L, Simonich M, Field JA, Tanguay RL. 2021. Behavior effects of structurally diverse per- and polyfluoroalkyl substances in zebrafish. *Chem Res Toxicol* 34(6):1409–1416, PMID: [34018735](https://doi.org/10.1021/acs.chemrestox.1c00101), <https://doi.org/10.1021/acs.chemrestox.1c00101>.
123. Tukker AM, Bouwman LMS, van Kleef RGDM, Hendriks HS, Legler J, Westerink RHS. 2020. Perfluorooctane sulfonate (PFOS) and perfluorooctanoate (PFOA) acutely affect human $\alpha_1\beta_2\gamma_2L$ GABA $_A$ receptor and spontaneous neuronal network function *in vitro*. *Sci Rep* 10(1):5311, PMID: [32210279](https://doi.org/10.1038/s41598-020-62152-2), <https://doi.org/10.1038/s41598-020-62152-2>.